Quaternary Science Reviews 268 (2021) 107111

Contents lists available at ScienceDirect

Quaternary Science Reviews

journal homepage: www.elsevier.com/locate/quascirev

Middle to Late Pleistocene faulting history of the Heerlerheide fault, Roer Valley Rift System, influenced by glacio-isostasy and mining-induced displacement

R.T. Van Balen [a, b, *], C. Kasse [a], J. Wallinga [c], H.A.G. Woolderink [a]

[a] Department of Earth Sciences, VU University Amsterdam, De Boelelaan 1085, 1081, HV Amsterdam, the Netherlands
[b] TNO - Geological Survey of the Netherlands, Princetonlaan 6, 3584, CB Utrecht, the Netherlands
[c] Netherlands Centre for Luminescence Dating & Soil Geography and Landscape Group, Wageningen University & Research, Droevendaalsesteeg 3, 6708, PB Wageningen, the Netherlands

ARTICLE INFO

Article history:
Received 23 April 2021
Received in revised form
19 July 2021
Accepted 22 July 2021
Available online 13 August 2021

Handling Editor: C. O'Cofaigh

Keywords:
Roer Valley Rift System
Heerlerheide fault
Trenching
Loess stratigraphy
Meuse terrace
Rocourt soil
Nagelbeek soil complex
Eifel volcanics

ABSTRACT

Faults of the Roer Valley Rift System (RVRS) are characterized by seismicity, scarps and displaced fluvial terraces, showing that they are active. The Heerlerheide fault is part of the southern boundary fault system of the RVRS, the Feldbiss fault zone (FFZ). During the late 19th and first half of the 20th century coal was mined in the subsurface south of the FFZ. As a result, general subsidence, sinkholes, and fault scarplets appeared on the surface. One of the induced fault scarps coincides with the location of the Heerlerheide fault, indicating that the upper part of the fault was reactivated by the mining. A trench was opened across the fault to study the mining-induced fault reactivation as well as the tectonic fault displacement history.

The Heerlerheide fault offsets a 340 ka Meuse river terrace overlain by loess and loess-like deposits of Eemian to Late Pleniglacial age, including the Rocourt soil, the Eben/Patina discordance and the Nagelbeek soil complex. At least three tectonic faulting events were reconstructed, which are most likely surface rupturing earthquakes. However, the two oldest displacements could represent multiple faulting events. The age of the youngest event is well constrained between 17 and 15 ka. The duration of the time interval between the penultimate and youngest events is at least 8 ky (the inter-event time is an important parameter for assessing seismic hazard). The vertical coseismic displacement of the youngest event was around ~0.25 m; the estimated moment magnitude is around 6.2. This event is more or less synchronous with the age of events found in other fault trench studies of the FFZ. The timing is roughly contemporaneous with surface rupturing earthquakes along the northern boundary fault zone of the RVRS, the Peel Boundary fault zone (PBFZ), and a phase of volcanism in the nearby Eifel area, suggesting a common mechanism. The timing also corresponds to the start of the glacio-isostatic forebulge collapse, which has been invoked before to explain earthquake events in the RVRS, and in northern Germany and Denmark.

Previous studies provided evidence for a Holocene surface rupturing earthquake with an offset of about 1 m at the Geleen fault in the Meuse valley on Belgian territory, taking place between 2.5 ± 0.3 and 3.1 ± 0.3 ka. The Geleen and Feldbiss faults on Dutch territory experienced faulting during the Late Glacial – Holocene. The incision and deposition history of a brook crossing these faults suggests an age around 7.5 ka for this event. However, in contrast, our results for the Heerlerheide fault show no evidence for Late Glacial – Holocene tectonic fault activity.

We also observed 0.34 m of vertical displacement of the base of the plough layer, which corresponds to the amount to what was observed at the surface during the mining in 1936, indicating that no fault motions have occurred afterwards, despite re-flooding of the mines and consequent surface rebound. However, the fact that the fault was reactivated by subsurface mining shows that it is a weakness zone in the subsurface, and therefore fault reactivation might occur due to still ongoing rebound. In contrast to

* Corresponding author. Department of Earth Sciences, VU University Amsterdam, De Boelelaan 1085, 1081, HV Amsterdam, the Netherlands.
E-mail address: r.t.van.balen@vu.nl (R.T. Van Balen).

https://doi.org/10.1016/j.quascirev.2021.107111

the tectonic fault displacement, the mining-induced offset was accompanied by downslope movement of the upper part of the hanging wall, resulting in splaying of the fault tip and crack formation.

1. Introduction

The Feldbiss Fault zone (FFZ) is the southern boundary fault zone of the Roer Valley Rift System (RVRS), located in the southern part of the Netherlands and neighbouring areas in Belgium and Germany (Figs. 1 and 2; Geluk et al., 1994; Van Balen et al., 2005). In the Dutch part of the RVRS, the FFZ consists of three faults, which are just a few km's apart: the Feldbiss fault in the north, the Geleen fault in the middle and the Heerlerheide fault in the south (Fig. 2). The faults are characterized by seismicity, scarps and displaced fluvial terraces, showing that they are active (Houtgast et al., 2002; Michon and Van Balen, 2005). The displacement histories of the Geleen and Feldbiss faults, including their past earthquake activity, have been studied using trenching in the Netherlands (Houtgast et al., 2003, 2005) and in Belgium (Camelbeeck et al., 2007; Vandenberghe et al., 2009; Vanneste et al., 2018). In the past there have been debates about the nature of tectonic fault displacements along the faults of the FFZ. Houtgast et al. (2003, 2005) favour a model of gradual, creep-like displacements. Interpretations in terms of surface-rupturing earthquakes have been put forward by Camelbeeck et al. (2007), Vandenberghe et al. (2009) and Vanneste et al. (2018). However, the details of the recent displacement history of the Heerlerheide fault are thus far unknown.

In the area south of the Feldbiss fault, coal-bearing Carboniferous strata have been mined in the late 19th and first half of the 20th century. The peak mining period was from 1930 to 1965; the last mine closed in 1974. The coal was mined using the longwall shearer technique, which involved the intentional collapse of abandoned, completed parts of the mines (Yavuz, 2004; Vervoort, 2016). This was applied on multiple, stacked mining levels. As a consequence of this method, subsidence occurred, resulting in fault scarplets (thresholds) and sinkholes at the surface (Heitfeld et al., 2016; Vis et al., 2020). These collapse features have been mapped during the mining, and many of them are still visible in the landscape, despite the levelling by agricultural land use (Fig. 3a and b). One of the induced fault scarp lineaments coincides with the location of the Heerlerheide fault (Fig. 3b and c), indicating that the upper part of the fault was reactivated by the mining. Re-flooding of the mines after closure caused regional uplift, which is still ongoing (Pöttgens, 1985; Caro Cuenca et al., 2013; Vervoort, 2016). This rebound counters only a fraction of mining induced subsidence, is gradual and not confined to the former mining concessions (Heitfeld et al., 2016). In 2018, a trench was opened across the Heerlerheide fault near Geleen (Fig. 3c,d,e), to study the mining-induced fault re-activation in vertical section. However, the trench was sufficiently deep (~4 m) to also assess the displacement history on a geological time-scale. Thus, the main objectives of this paper are to: 1) determine the Heerlerheide fault's tectonic and mining-induced displacement history based on trench observations, 2) compare it to the previous results for the nearby Feldbiss and Geleen faults of the same fault zone, and 3) to re-address the seismic or non-seimic nature of the fault displacements.

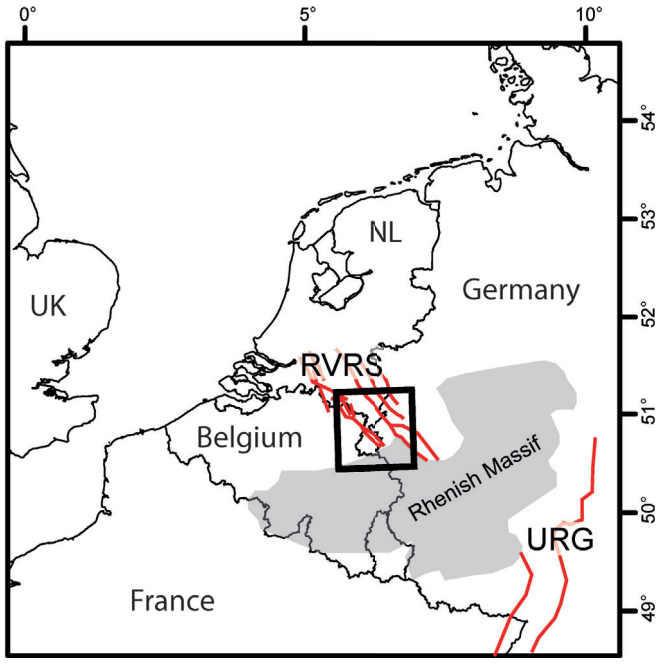

Fig. 1. Location of the study area in Northwestern Europe. RVRS = Roer Valley Rift. System, URG = Upper Rhine Graben. Coordinate system is in lat-lon using UTM projection.

2. Setting

2.1. Tectonics

The RVRS is situated in the northwestern part of the European Cenozoic Rift System (ECRIS; Ziegler, 1992; Michon et al., 2003). The last extension phase of the ECRIS started at the Oligocene-Miocene transition (Ziegler, 1992; Michon et al., 2003) and is still ongoing (Michon and Van Balen, 2005; Van Balen et al., 2005). The RVRS is part of a slowly deforming area with occasional earthquakes (e.g. Camelbeeck et al., 2007; Grützner et al., 2016; Kübler et al., 2017). The Roer Valley Graben (RVG) is located in the central part of the RVRS (Fig. 1). It is bounded by the Feldbiss Fault zone (FFZ) in the southwest and the Peel Boundary Fault zone (PBFZ) in the northeast. These two fault zones, and the continuation of the PBFZ into Germany, are at present the seismically most active faults in the rift system (Camelbeeck et al., 2007). The last damaging earthquake in the RVRS was the Roermond earthquake of 1992 (M_L5.8; M_S 5.4). It probably took place along one of the faults of the PBFZ (Van Eck and Davenport, 1994). Because of this earthquake, paleoseismological trenching studies were carried out in the decade following it (Van den Berg et al., 2002; Houtgast et al., 2003, 2005; Camelbeeck et al., 2007; Vandenberghe et al., 2009; Vanneste et al., 2018). An important result of these studies was that the time period around 15 ka, during the transition of the Late Pleniglacial to Late Glacial, has experienced an enhanced number of fault displacement events (Houtgast et al., 2003, 2005), many of which have been interpreted as earthquakes. This finding was recently confirmed by a new trenching study for the PBFZ (Van Balen et al., 2019). The concentration of fault displacement activity during the Late Pleniglacial to Late Glacial transition has tentatively been explained by the effects of glacio-isostatic movements, comparable to similar faulting events in northern Germany and Scandinavia (Houtgast et al., 2005;

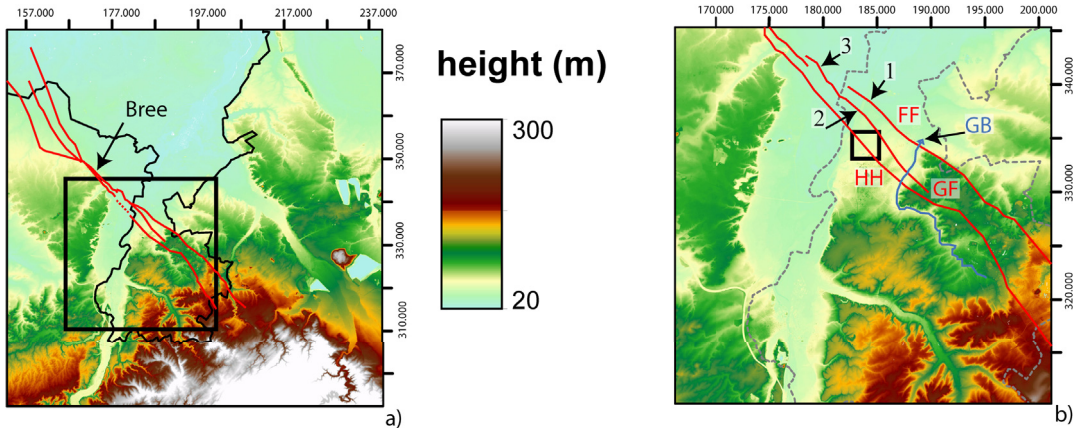

Fig. 2. Location and overview figures. Coordinate system is the Dutch National Grid (RD). a) Digital elevation model showing the large-scale topography around the study area. The red lines indicate the faults of the Feldbiss faultzone. Bree = location of Bree fault scarp. The position of a) is indicated in Fig. 1 b) Digital elevation model showing the topography around the study area. The fault trace of the Heerlerheide (HH), Geleen (GF) and Feldbiss (FB) faults of the Feldbiss fault zone are indicated by red lines. Locations of former trench studies are indicated by numbers: 1 = Houtgast et al. (2005), 2 = Houtgast et al. (2003), 3 = Vandenberghe et al. (2009). GB is the location of the Geleenbeek study by Ruijters et al. (2015). The position of b) is indicated in a). .(For interpretation of the references to colour in this figure legend, the reader is referred to the Web version of this article.)

Brandes et al., 2018; Van Balen et al., 2019; Müller et al., 2020). An important exception for the FFZ is a ~1 m surface rupturing event, dated between 2.5 ± 0.3 and 3.1 ± 0.3 ka, evidenced in a trench across the Belgian part of the Geleen fault (Fig. 2b; Vandenberghe et al., 2009; Vanneste et al., 2018).

From north to south, the Feldbiss fault zone in the Dutch part of the RVRS consists of three faults: the Feldbiss, Geleen and Heerlerheide faults (Fig. 2b). In the larger study area, the Geleen and Feldbiss faults behave as overstepping faults: their combined displacement rate, inferred from fault scarps and displaced Pleistocene fluvial terraces, is constant along strike: Towards the east, the offset along Geleen fault decreases and the Feldbiss fault dominates the displacement in the fault zone (Houtgast et al., 2002). In the western direction, in Belgium, the Geleen fault is at present the most active fault of the FFZ (Vandenberghe et al., 2009; Vanneste et al., 2018); it forms the very prominent Bree fault scarp (Fig. 2a; Camelbeeck et al., 2007). No studies have been performed yet for the recent tectonic activity of the Heerlerheide fault.

2.2. Coal mining-induced subsidence

Coal has been mined from 1926 to 1967 in the area immediately surrounding the location of the studied trench. The main mined areas extended from the south up to the Heerlerheide fault. However, because of the northward directed dip of the fault, the coal was also mined in the subsurface north of the surface trace of the fault, below the fault plane. Mining has taken place at five floor levels with depths ranging from about 400 to 800 m. The digital elevation data for the larger study area show NW-SE oriented scarplets, with offsets in the order of several decimeters (Fig. 3a and b). These represent surface expressions of relatively small, superficial normal faults caused by the intentional collapse used by the longwall shearer coal mining technique (Yavuz, 2004; Heitfeld et al., 2016; Vervoort, 2016; Vis et al., 2020). The most southwestern nearly continuous scarplet spatially coincides with the location of the Heerlerheide fault. The bundle of scarplets NE of the Heerlerheide fault scarp, and the also occurring sinkholes, can be explained by secondary faulting resulting from the combination of mining at depth and the northward inclination of the fault. The data on induced scarplets and sinkholes mapped by the engineers during the mining have been compiled by Heitfeld et al. (2016). For the larger study area, the scarplets are indicated in Fig. 4b. Fig. 4c shows the scarplets and sinkholes for the area directly surrounding the trench site. The Heerlerheide fault experienced a mining-induced vertical offset of about 0.4 m in 1936 (Heitfeld et al., 2016).

2.3. Stratigraphy

The stratigraphy exposed in the nearby former trenches across the Geleen and Feldbiss faults consists of fluvial gravel and sand deposits overlain by reworked loess (Houtgast et al., 2003, 2005). The fluvial deposits are part of a terrace staircase which has been carved in to the Mesozoic and Cenozoic bedrock by the Meuse river (Van den Berg, 1996; Van Balen et al., 2000). In both former trenches the fluvial deposits are correlated to the Caberg-3 terrace, which was dated by means of thermoluminescence (TL) to about 250 ka (MIS 8; Huxtable and Aitken, 1985; Van Kolfschoten et al., 1993; Van den Berg, 1996; Van den Berg and Van Hoof, 2001; Van Balen et al., 2000). The Heerlerheide fault trench in this study is located on a next higher terrace level, the Caberg-2 terrace. By assuming a climatic control on terrace development, the age of this terrace level is expected to be around 330 ka (Van den Berg, 1996; Van den Berg and Van Hoof, 2001; Van Balen et al., 2000). According to borehole data available at the geological survey (www.dinoloket.nl), also this terrace level is overlain by loessic deposits.

The loessic deposits are part of a belt of loessic sediments which have been lain down in an area extending from northern France, Belgium, southern Netherlands to the German Rhineland and beyond (e.g. Meijs, 2002; Schirmer, 2016; Lehmkuhl et al., 2016). The sources of the loess in the trenches were the nearby flood plain of the Meuse river, and the then exposed plains of the southern North Sea and English Channel (Lehmkuhl et al., 2016). After their deposition, the loess deposits have been reworked by local surface (runoff) processes such as sheet and shallow channel flow (Lehmkuhl et al., 2016).

Several studies have shown that within the loessic deposits major units, paleosols, tephra layers and discordances exist, that are comparable and contemporaneous over many hundreds of km (Meijs, 2002; Lehmkuhl et al., 2016; Schirmer, 2016; Zens et al., 2018). An example of an important and frequently occurring paleosol is the Rocourt soil (luvisol) complex which is of Eemian and Early Weichselian age (MIS 5; e.g. Haesaerts et al., 1999, 2016; Meijs et al., 2012). A second example is the Nagelbeek "tongued" horizon or Nagelbeek soil complex, which is a humic darkbrown greyish

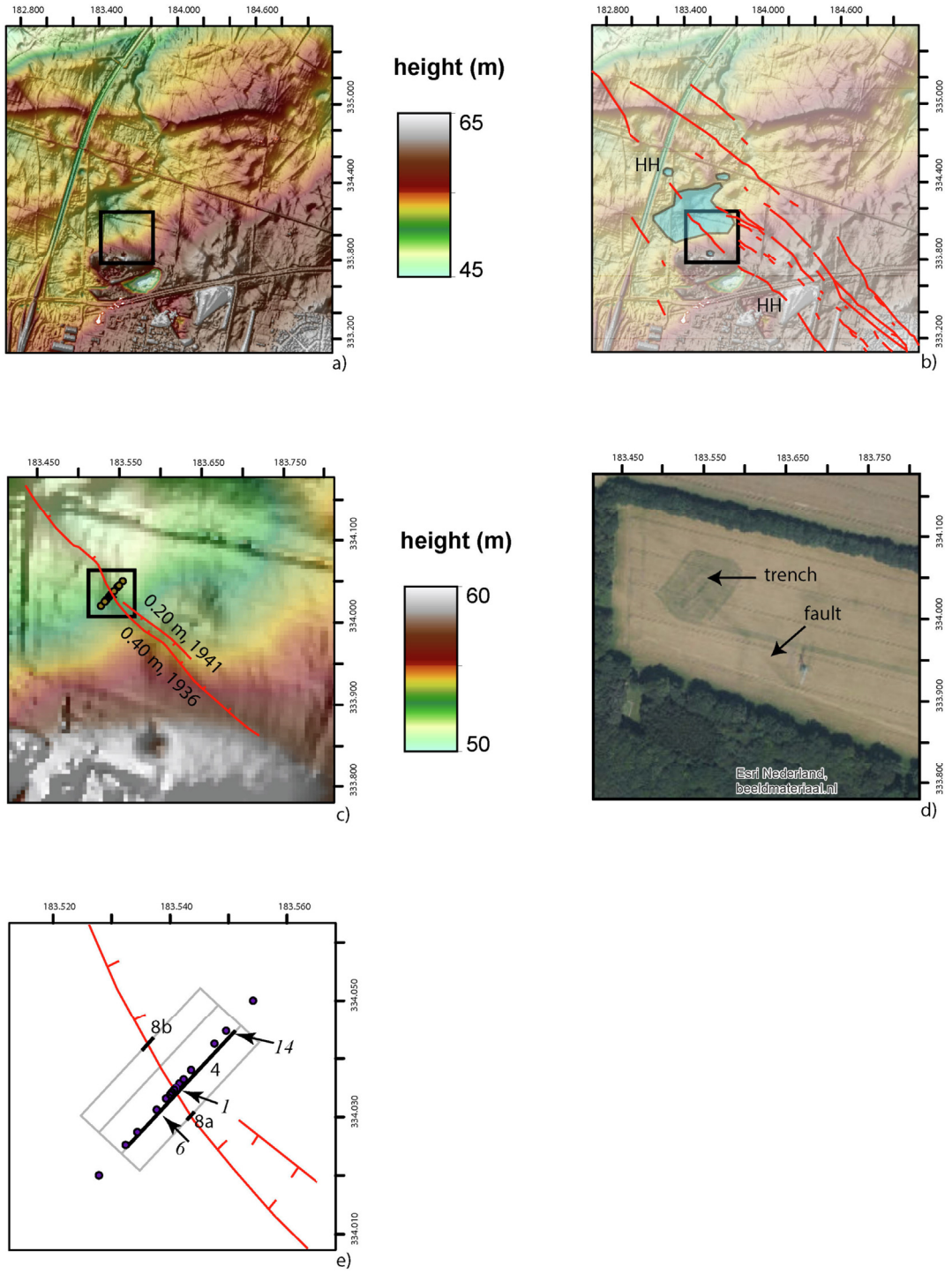

Fig. 3. a) Detail of the digital elevation model (with hill shading) showing the area surrounding the fault trench. The topography is characterized by scarplets and depressions caused by mining. The position of a) is indicated in Fig. 2b) b) Traces of fault scarplets mapped during the coal mining period (Heitfeld et al., 2016). Many of them are still visible in the present-day topography shown in a). The southern, nearly continuous scarplet coincides with the Heerlerheide fault (HH). Mining-induced sinkholes and an area of subsidence located in the study area are indicated in light blue. c) Digital elevation model of the study area. Red lines represent scarplets mapped during 1936 and 1941. Offsets and their dates as measured during the mining operations are indicated. Dots represent the location of drillings. The location of c) is indicated on a) and b). d) Aerial photograph of the study area presented in c), made after the trench was closed again. The former trench site is visible as a darker coloured rectangular patch. The distinct, NW-SE oriented trace is caused by soil wetness difference, caused by the Heerlerheide fault. e) Red lines show the locations of scarplets observed during the mining. The grey lines represent the outline of the trench. The dots are the drillings made before the trench was opened; italic numbers refer to specific drillings 1, 6 and 14 indicated in the profile of Fig. 4; other numbers indicate locations of Figs. 4 and 8a and b. The location of e) is indicated in c). (For interpretation of the references to colour in this figure legend, the reader is referred to the Web version of this article.)

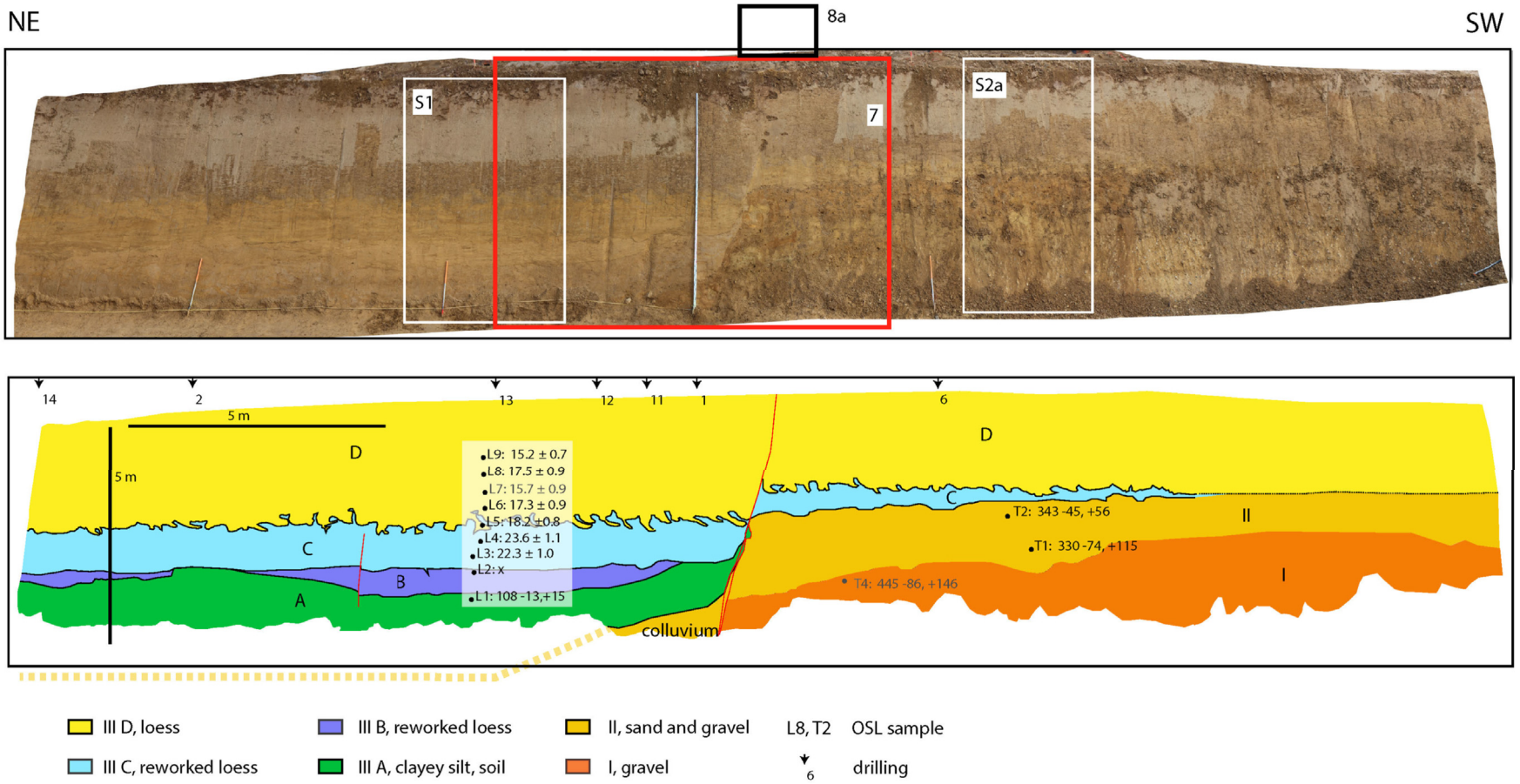

Fig. 4. The panorama photo and drawing of the main trench profile (note that the plough layer was removed before the trench was opened). The profile shows that the Heerlerheide fault was active since the deposition of the sand and gravel unit up to Present-day. See text for further discussion. The scale shows length along the inclined wall. Hanging wall is on the left, footwall is on the right. The trench wall is inclined by 45°. Red lines represent faults; L1-9 and T1,2, 4 are OSL samples with age results indicted in ka (L2 failed). L7 is not reliable and ignored in further interpretation. T4 has been projected on the section, since it was not taken in this profile. Drillings are indicated by arrows and labelled with numbers. The dashed orange line on the hanging wall indicates the approximate depth of the top of the sand and gravel unit based on the results of the drillings. A more detailed view of the OSL samples is in S1 and S2. 7 = the location of Figs. 7 and 8a = location of Fig. 8a. S1, S2a = location of Supplementary Figs. 1 and 2a. (For interpretation of the references to colour in this figure legend, the reader is referred to the Web version of this article.)

trundrasol with characteristic cryoturbations at its base (Juvigné and Wintle, 1988; Meijs, 2002, 2011, 2012; Pouclet and Juvigné, 2009; "E4 soil" in Zens et al., 2017, 2018). By correlation to the GRIP core (Johnsen et al., 2001), the age of the Nagelbeek "tongued" horizon is suggested to be 21 ± 3ka by Meijs (2011). Using all available regional age data (e.g. tephra's, ^{14}C, OSL), Zens et al. (2017) propose an age range of 23.2–25.6 ka for the Eltville tephra underlying the Nagelbeek soil complex, providing a *terminus post quem* for the formation of the tongued horizon. Loess deposition ends at the Late Pleniglacial – Late Glacial transition, and is followed by soil formation. Holocene soil formation usually overprints Bølling- Allerød soils (Lehmkuhl et al., 2016). See Discussion for further information on the loess stratigraphy in relation to the studied trench.

3. Methods

The position of the Heerlerheide fault was determined using the subsurface geological model "DGM" of the geological survey, available via (www.dinoloket.nl), and LiDAR-based digital elevation data (www.ahn.nl, version 2; e.g. Michon and Van Balen, 2005). As a third step, 15 drillings, each a few meters deep, were made to further constrain the exact location of the fault (Fig. 3c,e; Heitfeld et al., 2018). The drilling results are, however, coarse, and do not allow for detailed stratigraphic interpretations. Afterwards it turned out that the determined fault location corresponded to information from new aerial photographs (soil moisture differences and former trench position indicated on Fig. 3d) and to historical data of scarplet mapping by the mining engineers (Fig. 3b,c,e) (this information was not available to us before the trenching). The trench is located at the flank of an area of subsidence (Fig. 3b). The walls of the 30 m long and 4 m deep trench had a 45° slope. The trench was documented by means of dGPS, photos and drawings.

Away from the fault, on the downthrown block, 102 samples were taken in a profile with 5 cm resolution on the inclined trench wall (i.e. 3.54 cm vertical resolution). The samples were analysed for grain size and organic matter and carbonate content. The grain size subsamples were chemically pre-treated in order to remove organic matter and carbonates (Konert and Vandenberghe, 1997). Laser diffraction grain size analyses within the 0.15–2000 μm size range were performed with a Sympatec HELOS KR laser diffraction particle sizer. Organic matter and carbonate contents for subsamples were determined using a LECO thermogravimetric analyser 701 (Heiri et al., 2001). Weight loss (loss on ignition) was measured as a function of temperature from 25 to 1000 °C of 1–2 g of homogenized material. Because of the vaporized water content of the matrix, the first weight loss was at 105 °C. At 330 °C the less resistant organic material was burned; the remaining more resistant organic material was burned at 550 °C. The sum is here reported as total organic matter content. The subsequent heating to 1000 °C resulted in dissociation of carbonates.

3.1. Radiocarbon dating

A sample for 14C dating was wet sieved over a 200 μm mesh in the laboratory. Subsequently, bulk plant remains were extracted from the remaining sample material by use of a binocular microscope. The macro remains were (AMS) radiocarbon dated at the Beta Analytic laboratory (Miami, Florida) and calibrated using the Intcal13 curve (Reimer et al., 2013).

3.2. OSL dating

Twelve samples were taken to determine depositional ages using luminescence dating. Nine samples (L1-L9) were in fine-grained loessic deposits on the hanging wall and three samples (T1, T2, T4) in coarse-grained deposits on the footwall. Samples were taken by hammering metal tubes horizontally into the exposure, and transported to the Netherlands Centre for Luminescence dating at Wageningen University. Under subdued amber light conditions, samples were split with one part used for dose rate estimation (using gamma-spectrometry) and the other part for paleodose estimation. Depositional ages are obtained by dividing the palaeodose (amount of ionizing radiation absorbed by the mineral grains since burial, in Gy) by the dose rate (ionizing radiation absorbed by the mineral grains per thousand years, Gy/ka). Methods for both dose rate and palaoedose estimation are similar to those we used previously (Van Balen et al., 2019), and not repeated in detail here. Similar to our previous work, we use a combination of quartz OSL dating (e.g. Rhodes, 2011) for samples up to approximately 100 ka (L1-L9), whereas we adopt feldspar post-IR IRSL dating (Thiel et al., 2011) for older samples where quartz OSL signals are saturated (L1, L2, T1, T2, T4).

For dose rate estimation, we determined activity concentrations using gamma-ray spectrometry. Water contents as measured on the sampled material were used for determining water attenuation (between 6.6 and 20.9% by weight), and for the quartz OSL dated samples immediate burial to present depth was assumed for calculating the cosmic ray contribution. For the feldspar extracts gradual burial was assumed, and an additional contribution from internal potassium and rubidium is included following Kars et al. (2012). The assumed burial histories are based on preliminary OSL ages, indicating that the upper part of the sequence was deposited relatively rapidly, while there is a significant hiatus below.

For paleodose estimation, the quartz fraction of 125–180 μm was prepared using standard chemical methods, wet-sieving and magnetic separation (Porat, 2006). Equivalent dose measurements were made on small aliquots (1 mm, about 50 grains), using the SAR protocol (Murray and Wintle, 2003) with a preheat/cutheat combination of 260/220 °C and an early background approach (Cunningham and Wallinga, 2010). With this procedure, a given dose could be accurately recovered (dose recovery ratio 0.95 ± 0.02, n = 26), while the average D0 value was estimated at 64 ± 7 Gy (D0 is indicative of the onset of saturation, i.e., it characterizes the shape of the saturating exponential dose response curve). For each sample, measurements were repeated until at least 26 aliquots passed standard acceptance criteria. With the exception of sample L7, equivalent dose distributions showed little scatter (overdispersion according to the Central Age Model (CAM, Galbraith et al., 1999; provided in Table 1)) and were normally distributed. Hence we used a simple mean after rejection of outliers using an iterative procedure, removing those estimates deviating more than two standard deviations from the weighted mean. Results for sample L7 indicated a bimodal distribution, with the older component likely reflecting the time of deposition, and the younger component a post-depositional disturbance (e.g. mole hole). For samples L1, T1, T2 and T4 no reliable paleodose estimation was possible as absorbed doses were greater than 2*D0.

Potassium-rich feldspar extracts of 125–180 μm (L1) or 212–250 μm (T1, T2, T4) were obtained through standard chemical methods, wet-sieving, and density separation at ρ = 2.58 kg/dm3. A post-IR IRSL SAR sequence was used for palaeodose estimation (Thiel et al., 2011), with Preheat and Cutheat at 320 °C for 60 s, IR bleach at 50 °C for 100s, and post-IR IRSL readout at 290 °C for 500s. Other parameters and analysis were identical to those detailed in Van Balen et al. (2019). Dose recovery was determined to be 1.19 ± 0.04 (n = 12) which was deemed sufficient. No anomalous fading correction was used, as the post-IR IRSL signal used is expected to be (near) stable. It should be noted though that even a

Table 1
Summary of luminescence dating results (FS and Q denote paleodose estimation on feldspar or quartz fraction, respectively).

Sample	NCL code 31180-	Depth (m)	Paleodose (Gy)	Dose rate (Gy/ka)	Age (ka)	Mineral and reliability	Comments	(sub) unit
L9	09	1.30	45.3 ± 1.4	2.98 ± 0.11	15.2 ± 0.7	OK	Iterated De (CAM OD 14 %)	III D
L8	08	1.74	51.7 ± 1.8	2.95 ± 0.11	17.5 ± 0.9	Q, Likely OK	Iterated De (CAM OD 21 %)	III D
L7	07	2.08	47.8 ± 2.0	3.05 ± 0.11	15.7 ± 0.9	Q, Questionable	Iterative mean after manual cleaning of dataset (from OD 36 % to OD 15 %), admixture of 8 ka	III D
L6	06	2.39	53.4 ± 2.1	3.08 ± 0.12	17.3 ± 0.9	Q, OK	Iterated De (CAM OD 17 %)	III D
L5	05	2.67	54.5 ± 1.6	3.00 ± 0.10	18.2 ± 0.8	Q, OK	Iterated De (CAM OD 15 %)	III D
L4	04	2.94	66.1 ± 2.3	2.80 ± 0.09	23.6 ± 1.1	Q, Likely OK	Iterated De (CAM OD 19 %)	III C
L3	03	3.17	61.4 ± 1.9	2.76 ± 0.09	22.3 ± 1.0	Q, OK	Iterated De (CAM OD 17 %)	III C
L2	02	3.39	138.8 ± 6.8	2.91 ± 0.10	47.6 ± 2.9	Q, Questionable	Iterated De (CAM OD 46 %; 51 % > 2DO)	III B
L2	02					FS, not OK	Insufficient material for dating	III B
L1	01	3.71	171.8 ± 10.6	2.95 ± 4.2	58.2 ± 4.2	Q, Questionable	Iterated De (CAM OD 46 %; 51 % > 2DO)	III A
L1	01		414 (−48, +55)	3.83 ± 0.14	108 (−13,+15)	FS, Likely OK	General order fitting, no fading correction	III A
T1	10	3.42	970 (−217, +338)	2.94 ± 0.11	330 (−74,+115)	FS, Likely OK	General order fitting, no fading correction	II
T2	11	2.91	1097 (−139, +172)	3.20 ± 0.12	343 (−45,+56)	FS, Likely OK	General order fitting, no fading correction	II
T4	12	3.66	1494 (−290, +481)	3.36 ± 0.12	445 (−86,+146)	FS, Likely OK	General order fitting, no fading correction	I

small fading correction assuming a fading rate of 1 % per 'decade' would result in 30–50 % higher ages for these samples, with one sample even beyond the datable age range.

4. Results

A panorama photo and drawing of the southeastern trench wall are depicted in Fig. 4. The location of the trench, its topographic setting and relation to the fault scarplets mapped during the coal mining are indicated in Fig. 3c, d and e. The trench was opened after removal of the plough layer (Ap-horizon), which had to be preserved separately. However, exposures of the plough layer and underlying silt layer were still available for study next to the trench (locations indicated in Fig. 3e). Detailed photos and figures of these exposures are provided in separate figures, see below. In addition to the exposed stratigraphy, drilling results have been used to correlate the top of the two coarse grained units between the hanging wall and the footwall.

4.1. Trench stratigraphy

Based on texture, the sediments exposed in the trench were divided into 3 main lithostratigraphic units (Fig. 4). From base to top: unit I, a grey gravel sequence; unit II, a reddish and yellowish sand and gravel sequence; and an upper unit III, consisting of red-brown and yellow-brown silts.

The units I and II were only exposed in the footwall (apart from a small area immediately next to the fault); information about these units on the hanging wall was available from drillings (Heitfeld et al., 2018). Unit III was exposed all along the trench. Based on the presence of soils, discordances, cryoturbations and sedimentological characteristics (Figs. 5 and 6), this silt unit was subdivided into subunits A to D. All units and subunits have been sampled for OSL dating. In addition, silt unit III has been sampled for grain size and thermogravimetric analyses (TGA).

4.1.1. Unit I

This lowermost unit is a massive, sandy gravel deposit. The base of the unit was not exposed and not drilled. The top of the unit is at approximately 7.5 m depth on the hanging wall and 3 m on the footwall (drilling 6). The minimum thickness inferred in the trench is around 2 m and in the drillings about 2.7 m. No imbrication and no bedding was visible in the trench exposure. One ~10 cm thick coarse sand layer was present, which was sampled for OSL (sample T4).

The pebbles consist of quartzite, milky quartz and flint. Most gravels are sub-rounded; only some are sub-angular (e.g. the flints). In the trench the unit was fining upwards: at the base the average gravel size was about 10 cm (maximum size was around 40 cm) and at the top the average size was a few centimeters (maximum size was around 5 cm). The top of the gravel unit is wavy. At the contact with the overlying unit II large pebbles (up to ~10 cm) are present.

OSL Sample T-4 was taken from a ~10 cm thick layer of coarse sand in this unit (Fig. 4, Supplementary Fig. 2). The post-IR IRSL age for the gravel unit is 445 (−86,+146) ka (Table 1).

4.1.2. Unit II

This unit consists of a lower, yellow gravelly, silty-sand subunit and an overlying red gravelly, silty-sand subunit. In the trench the maximum combined thickness of the unit was about 2 m on the footwall. On the hanging wall the coarse drilling results indicate an average thickness of 3 m, with a range of 1.8–3.5 m.

The contact between the two subunits is irregular, wavy, just like the contacts with under- and overlying units I and III. Both subunits have a gravel layer at the top; the most pronounced is the upper one, at the contact with the overlying silty unit III (these gravel layers have probably resulted in stratigraphic misinterpretations for some of the gravel layers in the drillings by Heitfeld et al. (2018), who assign them to the top of the gravel unit I). The undulating contacts between the two subunits and to the over- and underlying units are probably due to periglacial loadings (Fig. 5f).

OSL Sample T1 was positioned in the middle of the yellow subunit (Fig. 4, Supplementary Fig. 1). The post-IR IRSL age is 330 (−74, +115) ka. OSL sample T2 is in the middle of the red subunit. The post-IR IRSL age of this sample is 343 (−45, +56) ka.

4.1.3. Unit III

The upper silt unit was well-exposed in the trench. It mainly consists of fine-grained deposits; the median grain size is 30–50 μm (Fig. 6). Based on erosional unconformities, soil horizons, and differences in colour and texture, the unit is subdivided in 4 subunits, A to D (Fig. 5a).

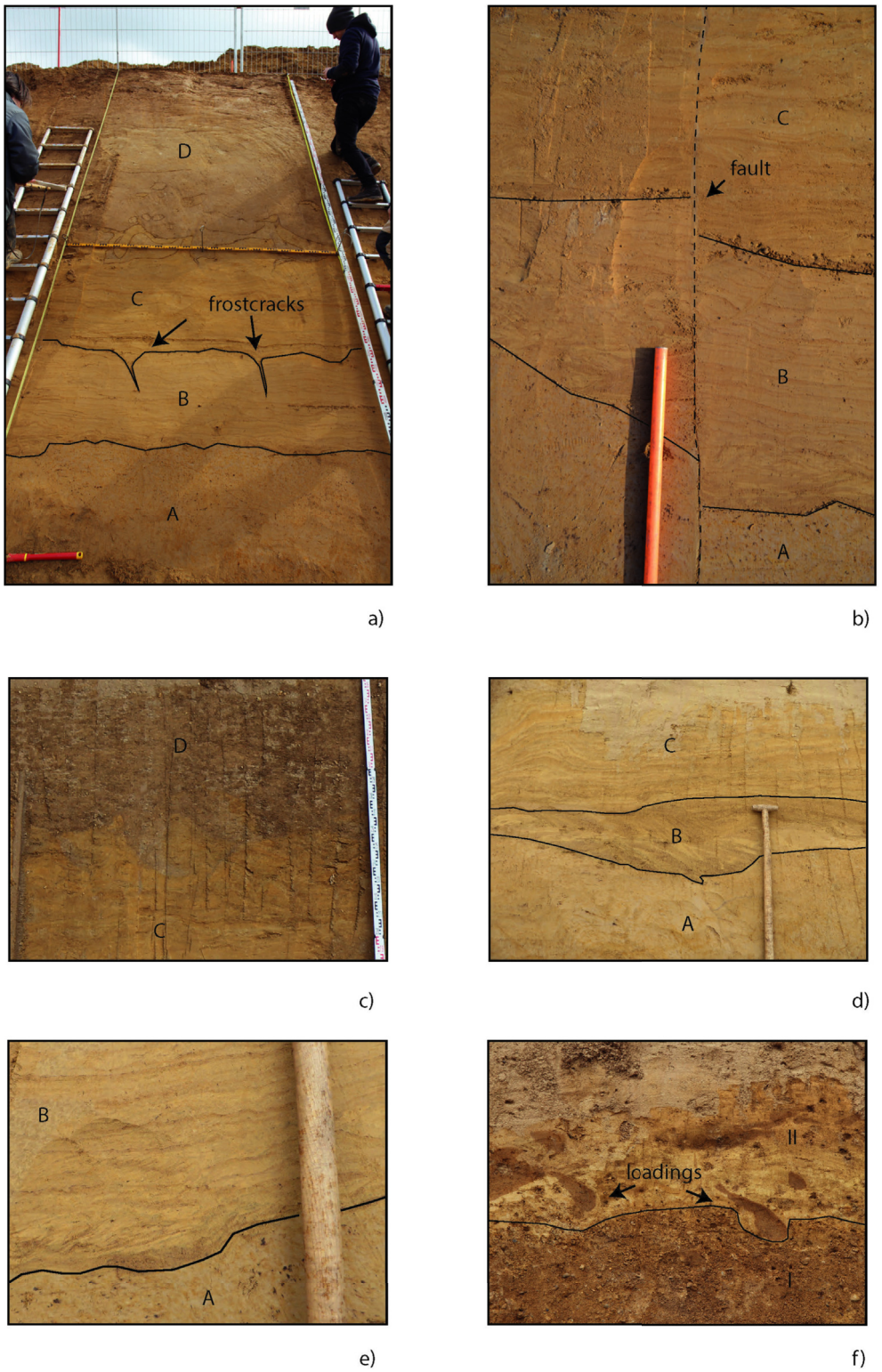

Fig. 5. Photos the units and subunits. a) overview of the subunits III A, B, C and D, in the middle part of the main trench profile, before the sampling. b) detail of subunits III A, B, and C along the secondary, antithetic fault. Pencil for scale. c) impression of subunits III C and D, with the Nagelbeek tongued horizon. d) subunits III A, B, and C in the western part of the main trench profile. e) detail of subunits III A and B at the main gully in the central part of the trench profile, showing small-scale cross-lamination. f) periglacial loadings in unit II.

4.1.3.1. Subunit III A. This subunit consists of clayey, blueish-grey, homogenous silt deposits with orange iron-oxide and dark-grey manganese oxide nodules (Fig. 6b, d and e). The median grain-size is 30–35 μm. The $CaCO_3$ and Org_{tot} have fairly low values of 0.85 resp. 1.6% weight. The subunit is at least 1.75 m thick (based on combining trench exposure information with data from drillings).

Subunit III A is interpreted as loess deposits in which a gley soil developed. These are likely primary (not reworked) loess deposits,

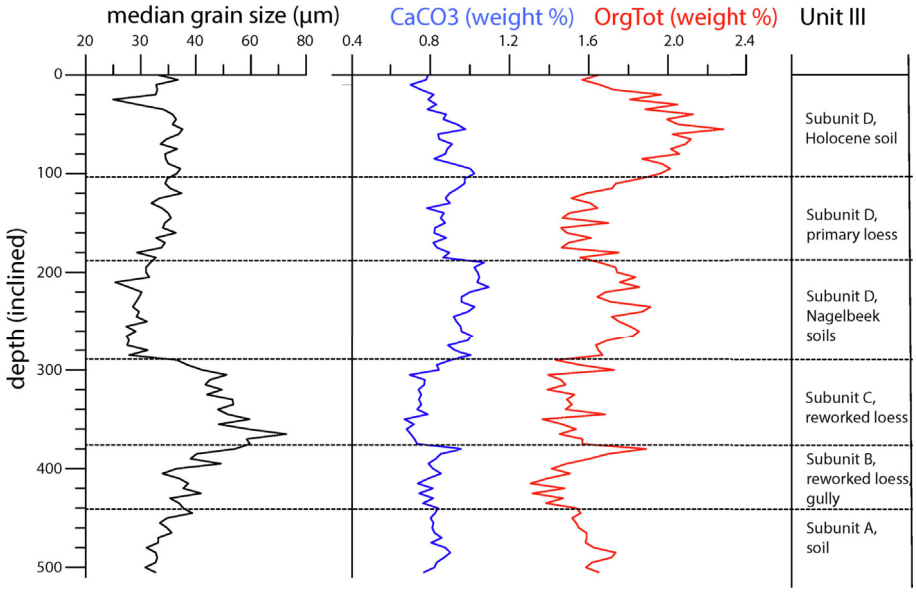

Fig. 6. Median grain size, carbonate and organic matter content for the units depicted in Fig. 4, sampled with 5 cm resolution along a depth profile on the inclined trench wall. The sampling locations are next to the OSL samples L1 to L9. Details are shown in Supplementary Fig. 1.

since they are homogeneous and no lamination nor bedding was observed. The subunit is present on the hanging wall, and in the fault zone, but it lacks on the footwall. OSL sample L1 yielded an unreliable quartz OSL result, but could be dated by post-IR IRSL providing an age of 108 (−13, +15) ka. The soil likely formed during the Eemian and Early Weichselian (MIS 5). Thus, deposition and soil formation occurred at the same time.

4.1.3.2. Subunit III B. This subunit also only occurs on the hanging wall. The base of the unit is gully-shaped, indicating it was formed by incision in to subunit III A (Fig. 4). The thickness of the subunit varies from 0 to 0.6 m. The internal, cm-scale layering conforms to the outline of the base of the subunit. In addition, small-scale cross lamination (Fig. 5e) was observed in this subunit, indicating (re) deposition of the loessic sediment by (shallow) flowing water. In the northern part of the trench a grit bed, i.e. a layer consisting of loess clasts, occurs. The grit deposit has foresets (~10 cm high), directed towards the fault (Fig. 5d). Cm-sized gravels occur at the top and base of the foresets. The median grain size of the silt deposits is around 40 μm (Fig. 6). The $CaCO_3$ and Org_{tot} values are fairly low, 0.8 resp. 1.4% weight. The top of the subunit is a discordance, characterized by sub-rounded, 3–4 mm size gravels.

One frost crack was present within subunit III B; 2 small frost cracks occur in the top, extending downward from the upper, gravelly discordance (Fig. 5a).

Subunit III B is interpreted to represent the infill of an incised gully with reworked loess that formed during cold climatic conditions.

OSL sample L2 taken near the central part of this subunit failed to produce reliable results. Nearly half of the quartz equivalent dose estimations was beyond the reliable range of 2D0, while there was insufficient material for feldspar post IR IRSL dating.

4.1.3.3. Subunit III C. This subunit consists of layered silt deposits with an average thickness of about 1 m on the hanging wall, and rapidly thinning on the footwall. The lower boundary with subunits III A and III B is a gravelly, sub-horizontal discordance. The wavy, cm-scale internal layering of the subunit consists of alternations of reddish brown, yellowish brown, and grey brown silts (Fig. 5b,c,d). A layer of small pebbles occurs in the upper part of the subunit. However, the gravel layer at the base contains more pebbles which are also larger. The upper boundary of the subunit is strongly deformed by cryoturbations. The subunit is coarser than subunit III B (Fig. 6); the median grain size varies between 40 (top) and 55 μm (base). The Org_{tot} and $CaCO_3$ values are similar to those of subunit III B.

The subunit is interpreted as reworked loess deposits, because of the larger grain size and laminated character.

OSL samples have been taken near the base (L3) and top of the subunit (L4). They resulted in ages of 22.3 ± 1.0 ka and 23.6 ± 1.1 ka, respectively, indicating that the subunit was deposited quite rapidly during the Late Pleniglacial (MIS 2).

4.1.3.4. Subunit III D. This fine-grained subunit consists of three parts. At the base it consists of strongly deformed silt deposits, with a dark grey colour (Fig. 5a and c). These deposits transition into the second, main part of the subunit, consisting of light grey -yellowish silts without stratification (only some vague large scale banding was observed), and with lower Org_{tot} and $CaCO_3$ values, and slightly larger median grain size (Fig. 6). Towards the top the colour changes to dark reddish brown and dark grey. In this part, the median grain size is around 35 μm, and the Org_{tot} and $CaCO_3$ values are around 2.0 and 0.9 wt %. The top of the subunit is the present-day surface. The maximum thickness of the subunit is around 3 m, being thickest on the hanging wall.

The basal part of subunit III D is strongly deformed, including the contact with subunit III C (Figs. 4 and 5a and c). The intensity of the deformations rapidly decreases upwards. The tongue-shaped, downslope (to the NE) directed deformations are best explained by cryoturbation (involutions). The lower median grain size values, the dark colour and the higher organic carbon content indicate that the basal part of subunit III D represents a soil. The overlying main part of the subunit is interpreted as aeolian silt deposits, i.e. primary loess (= not reworked) because of its homogeneous and massive character. The increase in organic content and change in colour in the upper part of the subunit is interpreted to be the Late Glacial - Holocene luvisol (Bt horizon). Note that the plough layer was not sampled and, therefore, not depicted in Figs. 4–6, because

this layer was removed before opening of the trench.

Five OSL samples were analysed for this subunit. Sample L5 at the base, in the lower part of a tongue, has an age of 18.2 ± 0.8 ka. Sample L6, and L8 in the middle of the subunit resulted in respectively 17.3 ± 0.9 ka, and 17.5 ± 0.9 ka. Dating of sample L7, in between L6 and L8, was problematic due to a bimodal equivalent dose distribution. Interpretation results in apparent ages of around 16 ka for time of deposition, and a bioturbated component of around 8 ka. However, both ages are regarded as not reliable and ignored in further interpretation. The highest sample, L9, near the base of the luvisol resulted in an age of 15.2 ± 0.7 ka. All together, the OSL results show that the subunit was deposited in a short time interval during the Late Pleniglacial. A ^{14}C sample from bulk organic material from the basal part of a cryoturbation tongue resulted in a ^{14}C age of 31790±180 BP (corresponding to an Intcal13 calibrated age of 36149–35242 cal BP). This result shows that the organic material in the tongue-shaped cryoturbations consists of reworked organic deposits, and is not derived from contemporaneous vegetation.

4.2. Faults

The main fault offsets all stratigraphic units, and can be traced up to the surface of the trench (Figs. 4 and 7). In a separate exposure next to the trench, the fault was found in the base of the plough layer (Fig. 8a). The average fault dip is 75° towards the northeast (050/75). At the base of the trench wall the fault is a single plane. Further upwards it splays, offsetting subunit III A, and juxtaposing it against the gravel and sand unit II on the footwall. Here the fault consists of multiple branches and the fault core is thicker. At the level of subunit III C and the base of subunit III D the fault has a single plane. At approximately 1 m below the original surface (0.6 m below the top of the trench surface) the fault splays again (Fig. 7). One splay has the same dip and offset as the fault at larger depth. The other splay dips and offsets in the opposite direction (Figs. 7 and 8a). These upper fault-splays offset the plough layer by about 0.35 m. A wedge-shaped part of the plough layer is present in the top of the profile enclosed by these fault-splays (Figs. 7 and 8).

In the hanging wall, a small antithetic fault offsets the subunits III A, B, and C (Figs. 4 and 5b). This fault could not be traced towards the surface (despite the stratification) nor towards the base of the trench.

5. Discussion

5.1. Correlation to the regional stratigraphy

The massive sandy gravel deposits in unit I are fining upwards. According to regional drillings (www.dinoloket.nl), the deposits are regionally extensive, with a fairly constant thickness. The unit contains sub-rounded pebbles consisting of (Revinien) quartzite and flint, which are characteristic for deposits formed by the Meuse river. Based on these characteristics, the unit is interpreted as a Meuse terrace deposit (e.g. Van den Berg, 1996), comparable to the former trenches across the Geleen and Feldbiss faults (Fig. 2b; Houtgast et al., 2003, 2005) and in line with the geomorphological data, see below. The overlying unit II consists of gravelly, silty-sand deposits. This unit is also regionally extensive; it is present in the trench (exposed and in drillings) and in the regional drillings, indicating that it is not a local colluvial or slope deposit. The gravel beds in this unit indicate that the (original) depositional environment of this unit is also fluvial. In addition, the occurrence of this unit on top of the gravelly unit I is in agreement with the fining upward trend of pebbles observed in the latter. Therefore, we interpret unit II to essentially represent the upper part of Meuse river terrace deposits. However, unit II is clearly multi-genetic: It is characterized by peri-glacial loadings (Fig. 5f; also internally), thin gravel beds are present, indicating erosional phases, and clear fluvial stratification is lacking. Based on geomorphological position, units I and II can be correlated to the Caberg-2 terrace (Van den Berg, 1996; Houtgast et al., 2003), which, by correlation to MIS 10, has an estimated age of around 330 ka (Van den Berg, 1996; Van Balen et al., 2000). Taking into account the uncertainty in the OSL ages, the age ranges for the OSL samples in the units I and II are in agreement with this age estimate. We interpret the red colour of the upper part of unit II to be the result of (multiple cycles of) soil formation. This hypothesis is supported by the large age difference with the overlying silt unit III, indicating a long period of non-deposition and/or erosion.

The silt unit III overlying the terrace is much younger. The blueish grey fine silt subunit III A can, because of its characteristics and OSL age constraints, be interpreted as a soil of Eemian and Early Weichselian age (MIS 5), which can be correlated to the Rocourt soil (Meijs, 2002; Schirmer, 2016; Lehmkuhl et al., 2016). At our study site the soil is a gleysol, whereas the Rocourt soil is typically a luvisol. This difference can be explained by wet conditions at our study site.

Subunit III B, the infilled gully, could not be dated, and cannot be correlated to previously described loess units. Based on the small gravels and frost cracks and on the OSL ages of overlying subunit III C, the discordance situated at the top of subunit III B, and locally, where B is absent, on top of subunit III A, can be tentatively correlated to the regional Patina discordance (named after wind-polished, patinated pebbles; Meijs et al., 2012). This discordance is also known as the Eben discordance (Schirmer, 2016); its age is slightly younger than the Eltville tephra (Zens et al., 2017). Sediments surrounding this tephra have been dated many times at many localities in Western Europe, using different techniques (e.g. Juvigné and Wintle, 1988; Pouclet and Juvigné, 2009; Schirmer, 2016; Zens et al., 2017). Bayesian age modeling yields a tephra deposition age between 23.2 and 25.6 ka (Zens et al., 2017). However, we did not encounter the characteristic Eltville tephra in the trench.

Subunit III C resembles the Kesselt layer of Schirmer (2016), which is described as an up to 1 m thick unit consisting of reworked loess deposits, redeposited as a variegated mixture of loess, decalcified loess and soil material, with sand and gravel. Elsewhere, the Kesselt layer overlies the Eltville tephra, see above. The OSL dates of c. 23 ka of subunit III C are in agreement with this correlation. Nearby, in Romont, the reworked sediments of the Kesselt layer were OSL dated to 25.0±2.1 ka (Zens et al., 2018).

The basal part of subunit III D, a soil characterized by tongue-shaped cryogenic deformations, can be correlated to the regional soil complex of the Nagelbeek “tongued” horizon. Our OSL age results, 18.2±0.8 ka (L5) at the base, 17.3±0.9 ka (L6) in the middle and 17.5±0.9 ka (L8) just above this subunit, are in agreement with the proposed ages for the horizon (e.g. Meijs, 2011; Zens et al., 2017).

The main part of subunit III D consists of aeolian, unstratified loess, and can therefore be correlated to the Brabant loess (Meijs, 2002, 2011, 2011; Schirmer, 2016; Zens et al., 2017), which is in agreement with the age of 15.2±0.7 ka for OSL sample L9. Like elsewhere, the upper part of the Brabant loess, and thus subunit III D, has been altered by Late Glacial - Holocene luvisol formation. According to Jongmans et al. (2013), clay illuviation was only possible in the Netherlands during the Late Glacial; the Holocene climatic conditions are less suitable for the clay-illuviation

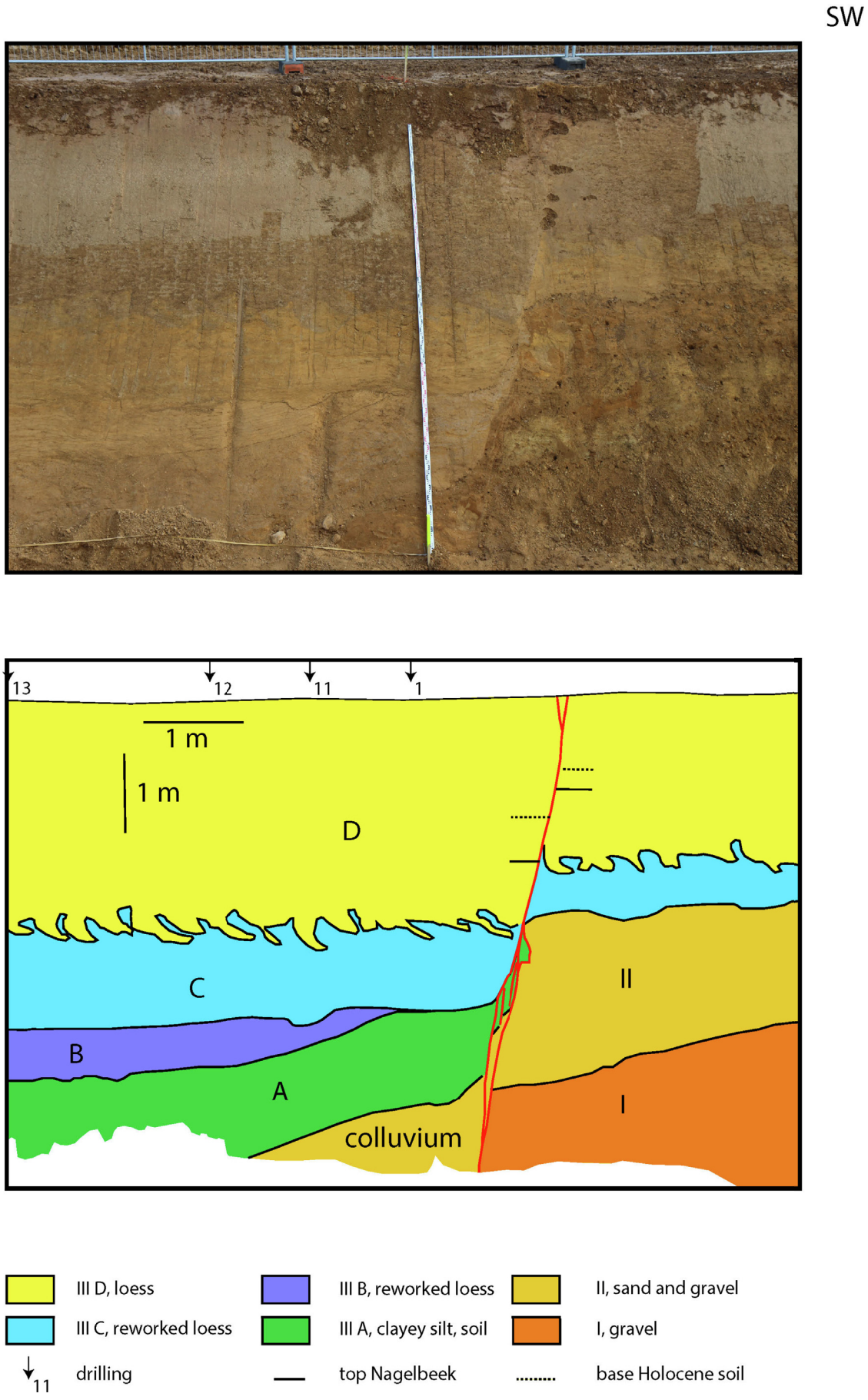

Fig. 7. Detailed photo and drawing of the main fault (note that the plough layer was removed). The dashed line represents the base of the Late Glacial - Holocene luvisol and the full line corresponds to the top of the Nagelbeek soil horizon (could not be determined for the rest of the trench profile). The Heerlerheide fault splays in the lower part and in the uppermost part.

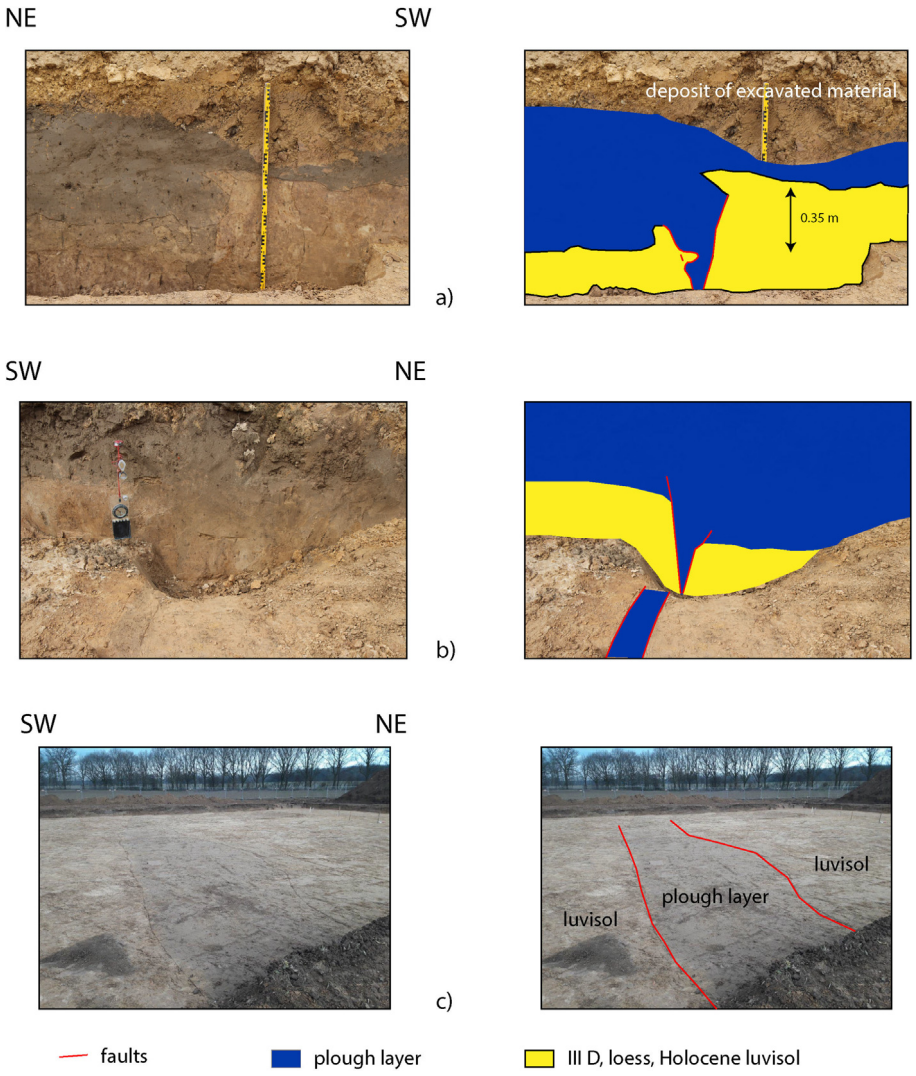

Fig. 8. Photos and drawings presenting the fault in and just below the plough layer, showing displacement of the Late Glacial - Holocene luvisol and the base of the plough layer. The locations of the subfigures are shown in Fig. 3e a) The base of the plough layer (Ap-horizon) is displaced by about 0.35 m. A crack opened in the top of the fault; it is filled with plough layer sediment. Pieces of cokes (product of heated coal) and a pebble were present in the crack filling. Location indicated by 8a in Figs. 3e and 4. The section is vertical. b) Similar situation as in a), on the opposite side of the trench (northwestern trench wall). In the foreground is the trace of the crack on the horizontal section. Location indicated by 8 b in Fig. 3e c) View of the study area after removal of most of the plough layer, but before opening of the trench. Darker colours delineate part of the plough layer that subsided in between the main fault (left) and a secondary fault. . (For interpretation of the references to colour in this figure legend, the reader is referred to the Web version of this article.)

process.

5.2. Sequence of events

Based on the reconstructed depositional environments and the observed fault offsets of the different stratigraphic units, we are able to reconstruct the sequence of events (Fig. 9). The event history was derived by considering Fig. 7 as the end −result, i.e. the accumulation of all depositional and faulting events starting from terrace deposition. We have been able to make the reconstruction by stepwise removing the deposits and by un-displacing them, starting from Fig. 9i (based on Fig. 7). However, we present the results forward in time. Below we first summarize important observations and their implications for the reconstruction.

1) the top of the fluvial terrace deposits (units I and II) is subhorizontal, except on the hanging wall directly next to the fault. This exception could indicate either a fault splay (not visible), fault propagation folding, or a colluvial wedge. If it is a colluvial wedge, then this implies a paleo-fault scarp.
2) subunit III A is present on the hanging wall and in the fault core, but not on the footwall. This could imply complete erosion of this subunit on the footwall. But on the other hand, it could also imply that the subunit was not deposited on the footwall. In that case, subunit A was deposited on the hanging wall against a fault scarp. In this scenario the soil in this subunit can be correlated to the soil in the top of unit II on the footwall (although that soil is the result of many soil-formation cycles). This seems to us the most likely hypothesis, as it is in agreement with observation 1). In addition, if subunit III A would have been completely eroded from the footwall, we would expect to find abundant loess clasts as erosion products in the overlying sedimentary units III B and III C. Although such clasts do occur, the small quantities make it unlikely that large-scale erosion took place.

3) because subunit III A is present in the fault core, the fault must have displaced and splayed after deposition and soil formation in this subunit, but before deposition of subunit III C, as that subunit is not present in the fault core.
4) the thickness of subunit III C gradually decreases from hanging wall to footwall. This implies the unit was deposited on a slightly sloping levelled surface and no fault displacement took place during deposition.
5) the basal part of subunit III D, the Nagelbeek soil complex, has a nearly constant thickness. This implies the unit was deposited on a nearly levelled surface and no fault displacement took place during deposition.
6) the top of the Nagelbeek soil complex has more vertical displacement (0.60 m) than the base of the Late Glacial - Holocene luvisol (0.34 m). The base of the Late Glacial-Holocene soil has nearly the same displacement as the base of the plough layer (0.35 m, Fig. 8a), which in turn has about the same magnitude as what has been measured during the mining (0.4 m, Fig. 3c). The implication is that about 0.25 m tectonic fault displacement occurred after the Nagelbeek soil complex was formed, but before the Late Glacial – Holocene soil formation.

The reconstruction starts with the last stage of the deposition of fluvial terrace deposits at about 340 ka (MIS 10), shown in Fig. 9a. This should be close to the abandonment age of the terrace. During the next long time step, between 340 and 130 ka (from MIS 10 to the transition of MIS 6–5), depicted in Fig. 9b, the fault has displaced and a colluvial wedge was deposited against the paleoscarp. The formation of the colluvial wedge implies some erosion on the footwall occurring at the same time. The coarse drilling results on the hanging wall provide a variable depth to the top of unit II of about 4.5 m and a thickness of around 3 m. On the hanging wall the thickness of unit II is about 2 m, implying ~1 m of erosion. The reconstructed vertical offset of ~2.7 m (Table 2) is based on the height difference between the top of unit II on the hanging wall and the restored top on the footwall, corrected for younger displacements.

During the next step, during MIS 5 and shown in Fig. 9c, subunit III A was deposited against the fault scarp. Soil formation took place in this subunit and in unit II on the footwall. Because of the gravelly discordance with subunit III C and the incision by subunit III B, the top of subunit III A must have been higher than what is preserved.

Subsequently, fault displacement takes place after deposition of subunit III A, but before formation of the Patina discordance and deposition of subunit III C (Fig. 9d). The new steep branch developing in this stage could be either a result of the new free surface (reset by erosion) or of the presence of the colluvial wedge. The vertical offset of ~0.5 m is based on the offset of unit III A, corrected for younger displacements. Because subunit III C has a gradually decreasing thickness no fault scarp and also no faulting occurred during its deposition (25–20 ka; Fig. 9e).

The basal part of subunit III D, the Nagelbeek soil complex, has a constant thickness on the footwall and hanging wall, implying no faulting and hardly any relief during this time period (Fig. 9f). However, the cryogenic tongues are clearly directed towards the NE, implying at least several degrees of slope during periglacial conditions.

During deposition of the remainder of subunit III D, 0.25 m of tectonic displacement occurred (Fig. 9g). Late Glacial - Holocene soil formation took place afterwards (Fig. 9h) and was followed in recent times (1936) by 0.34 m–0.4 m mining-induced faulting (Fig. 9i). Afterwards, the fault scarplet was levelled by ploughing. The amount of displacement is the same as what has been mapped during the mining, showing that in the past decades no fault displacement has occurred. The mining-induced offset was accompanied by downslope movement of the upper part of the hanging wall, resulting in splaying of the fault tip and crack formation. A slope is still present in the landscape (Fig. 3a,c).

A summary of determined fault offsets is listed in Table 2.

5.3. Paleoseismological implications

The oldest reconstructed faulting episode is not very well constrained in time, it occurs somewhere between 340 and 130 ka. In addition, there is not much evidence for the type of fault movement. The colluvial wedge and paleo-fault scarp indicate that displacement likely has been abrupt, but it does not provide indications for the number of events. The base of the colluvial wedge would represent the event layer of the oldest displacement. But it was not exposed. The timing of the next faulting episode in our trench is slightly better constrained, between 110 and 25 ka. The sharp fault strands through the part of subunit III A in the fault core are indicative of abrupt fault displacement, favouring an interpretation as one or more surface rupturing earthquakes. But unfortunately, due to strong erosion by the base of subunit III C, it cannot be established that the observed offset is the result of one or multiple events. Other displacement type indicators (e.g. a colluvial wedge) are lacking. The event layer corresponds to the boundary between subunits IIIA/B and subunit C, the regional Patina discordance. Erosion during formation of this discordance can explain the lack of other displacement indicators. The reconstructed amount of offset is ~0.5 m (Table 2), which, if it was one event, would imply a moment magnitude of about 6.5 (Wells and Coppersmith, 1994). The final tectonic fault displacement is reconstructed to amount to ~0.25 m and is well constrained to the period 17–15 ka (Table 2). This short period of time suggests that it was a surface rupturing earthquake, and based on the offset it indicates a moment magnitude of about 6.2. Unfortunately it was not possible to identify the event horizon or possibly associated colluvial wedge in the massive and pedogenized loess of subunit III D. The larger amounts of offset for the two oldest events compared to the youngest indicates that the older ones might represent multiple faulting events. The results do not allow determining precise inter-event times, which is an important parameter for assessing seismic hazard. Only a minimum duration of the time-interval separating the last and penultimate events can be concluded, which is 8 ky (25–17). In the future, a new trench situated on a younger Meuse terrace might give such results.

5.3.1. Paleoseismological correlation to other trenches

The FFZ has been active since at least Early Mesozoic time, during several rifting and inversion episodes of the RVG (e.g. Geluk et al., 1994; Deckers et al., 2021). Therefore, considered at a crustal scale, the FFZ is a prominent weakness zone, whereby the different constituting faults represent its branching towards the surface. In the Dutch part, the FFZ comprises from north to south the Feldbiss-, Geleen and Heerlerheide faults (Fig. 2a and b). Further west, in the Meuse valley, the continuation of the Geleen fault in Belgium is the Neeroeteren fault; the Heerlerheide fault continues as the Rotem fault (Vandenberghe et al., 2009; Vanneste et al., 2018; Deckers et al., 2021). The two faults join to form the Bree fault scarp further west (Fig. 2a). All these faults have been studied in the past using trenches (Figs. 2b and 10), except for the Heerlerheide/Rotem fault. Our study allows for the first time a comparison.

The one or more earthquake events during the time-period between 340 and 130 ka found in the Heerlerheide trench are synchronous with the oldest event documented in trench 4 near Bree (Fig. 10; Camelbeeck et al., 2007; Vanneste et al., 2018) and in the Geleen fault trench of Houtgast et al. (2003). However, the age

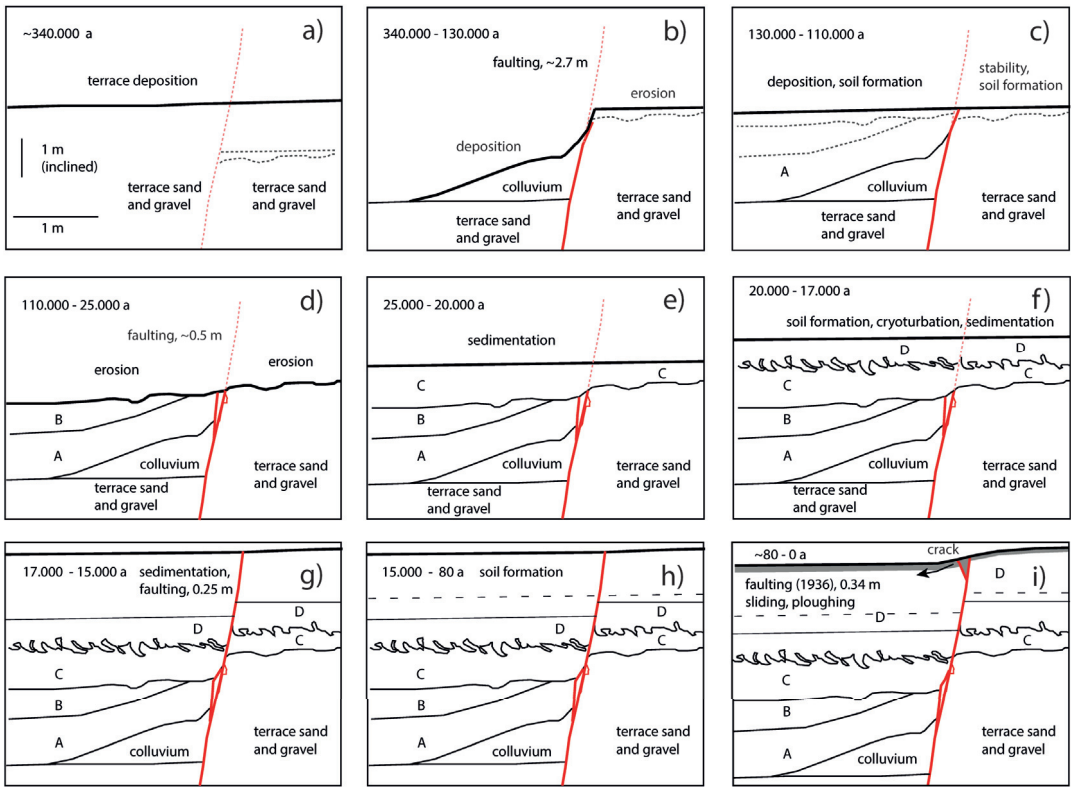

Fig. 9. The reconstructed sequence of events. The schematic reconstructions are based on Fig. 7. The thick black line represent the surface. a) deposition of the terrace sand and gravel deposits (units I and II) by the Meuse river at 340 ka. b) after abandonment by the Meuse, down faulting of the terrace, erosion of the footwall and deposition of a colluvial wedge against the scarp occurred. The formation of the colluvial wedge likely indicates sudden, abrupt fault movement. c) Following deposition of the colluvial wedge, loess-like fine-grained sediments are deposited against the scarp (subunit III A), in which a luvisol is formed. Soil formation also affected the upper part of the fluvial terrace deposits. d) the top of subunit A is incised. Subunit B, consisting of reworked loess −like sediments, is deposited in the incised gully. A next phase of erosion erodes the top of the gully fill, subunit B, and again, the top of subunit A, forming one levelled surface characterized by small pebbles, the Patina/Eben discordance. Sometime before the erosion, before or after deposition of subunit III B, fault displacement created a steep, new branch in the upper part of the fault; a part of subunit III A is from now in the core of the fault zone. Surface offset is levelled by erosion. Faulting might have been abrupt, because of the straight and clear fault traces, but no colluvial wedge has been preserved. e) Subunit C is deposited on a slightly sloping surface as evidenced by the gradual thinning from hanging wall to footwall. During deposition it was not affected by faulting. f) the basal part of unit D was deposited and cryoturbated (Nagelbeek soil complex), with similar thickness on hanging wall and footwall. This implies no fault movement during its deposition. g) the upper part of subunit D is thinner on the footwall then on the hanging wall, indicating a fault displacement event occurring during deposition. A colluvial wedge associated with this displacement could not be identified in the massive and pedogenized loess. h) the Late Glacial- Holocene luvisol is formed. i) the plough layer is displaced by mining-induced faulting, and a small crack formed in the tip of the fault, indicating sliding of the plough layer. Afterwards, the scarp is levelled by ploughing and soil erosion. The base of the Late Glacial- Holocene luvisol is as much displaced as the plough layer is.

constraints are not good enough to make a detailed correlation.

For the inferred event(s) between 110 and 25 ka a detailed correlation to other trenches is also not possible due to the large time interval. Nevertheless it seems likely that there have been multiple events: Houtgast et al. (2005) found two mass wasting events (solifluction) dating from this time period; indicating two earthquake events for the Feldbiss fault. For the Geleen fault, Houtgast et al. (2003) documented three potential earthquake events, the oldest evidenced by a colluvial wedge, and the younger two by mass wasting (solifluction). For the Geleen fault at the Bree scarp, three consecutive colluvial wedges were formed after 101 ± 10 ka and before the Last Glacial Maximum, indicating individual displacements between 0.3 and 1 m (Vanneste et al., 2018).

The surface rupturing event during the 17−15 ka time interval is well correlatable: it also occurs in the results of every trench study for the FFZ (Fig. 10). For the Felbiss fault near Born (Fig. 10), a 0.21 m offset occurred during the deposition of a unit dated between 22.8 ± 1.6 and 13.5 ± 1.0 (Houtgast et al., 2005). For the Geleen fault near Born (Fig. 10) an earthquake during this period is evidenced by fluidization structures (dikes, flames) dated at about 15 ka (Houtgast et al., 2003). According to Houtgast et al. (2003), no fault offset occurred during this event. Instead, the sequence with fluidization structures is covered by a new sequence lacking fluidizations, but with a similar, slightly younger, age. Because the two sequences are faulted by the same amount, Houtgast et al. (2003) conclude that a small time-interval occurred between earthquake fluidization and surface rupture, during which the thin, non-fluidized sediment sequence was deposited. However, from their profiles it is clear that some fault splays terminate exactly at the boundary between the two sequences, which indicates that this boundary could represent an event horizon, evidencing that a surface rupture occurred during fluidization. The faulting affecting both sequences would then represent a younger event. In the Meuse valley, the penultimate event at the Geleen fault (Rotem-2,

Table 2
Fault displacement episodes. Vertical displacements are corrected for younger offsets.

Time interval	Vertical displacement
1936	0.34 (trench) - 0.4 m (surface)
17−15 ka	0.25 m
110- 25 ka	~0.5 m
340-130 ka	~2.7 m

Fig. 10) is dated between 18.2 ± 1.3 ka and 15.9 ± 1.1, its offset is about 0.4 m (Vandenberghe et al., 2009; Vanneste et al., 2018). For the trenches along the Geleen fault at the Bree scarp, Vanneste et al. (2018) suggest an age close to the last Glacial Maximum (19–14 ka) for the penultimate event, with an offset of 0.33 m.

We did not find evidence in the Heerlerheide trench for tectonic Late Glacial or Holocene displacement at the Heerlerheide fault, because the base of the Late Glacial-Holocene luvisol and the base of the plough layer show the same amount of displacement. This contrasts with the results of the trenches at the Feldbiss and Geleen faults. In the Meuse valley trenches across the Geleen fault, the age of the youngest events was well constrained. The last event was between 2.5 ± 0.3 and 3.1 ± 0.3 ka and had an offset of about 1 m (Vanneste et al., 2018). The age of the youngest event for the Geleen fault along the Bree scarp is not well constrained, but should have occurred during the later part of the Holocene because of displaced soil horizons. At the fault the offset is 0.12 m, but at the larger scale displacement is 0.8 m if flexuring is taken into account (Vanneste et al., 2018). At the Feldbiss fault near Born a vertical displacement of 0.63 m has taken place, postdating the youngest loess deposit (dated at 13.8 ± 1.0 ka; Houtgast et al., 2005). For the Geleen fault at Born, the base of the primary loess deposits (the upper part of our unit III D) is flexed (Houtgast et al., 2003), but no faults could be discerned, which might be due to the homogeneous character of the deposits, or the limited amount of displacement (i.e., flexing as an effect of fault-propagation folding). These Late Glacial-Holocene displacements at the Feldbiss and Geleen faults cannot be attributed to mining-induced reactivation, because they are located outside the former coal mining area. Further constraints for the timing of these fault displacements can potentially be derived from an incision and infilling event by the Geleen-beek, a brook which crosses these faults (Fig. 2b), just downstream of the Feldbiss fault. The incision and infilling of this brook were OSL-dated. The 1–3 m deep incision into loamy alluvial fan deposits postdates 8.1 ± 0.7 ka, the subsequent fluvial sand infilling started before 7.0 ± 0.5 ka (an additional sample resulting in 7.7 ± 0.6 ka is also available, but is not preferred because of archeological arguments; Ruijters et al., 2015). The rapid incision followed by sedimentation, and the slightly higher fluvial energetic conditions implied by the increase in grain size, cannot be attributed to human impacts or to climate change, leaving the effects of an earthquake around 7.5 ka as the most likely explanation (Ruijters et al., 2015).

5.3.2. The impact of glacio-isostasy on faulting during the Late Pleniglacial-Late Glacial transition

A concentration of fault displacements in the RVRS during the Late Pleniglacial-Late Glacial transition determined in trenches was already noted by Houtgast et al. (2005). They attributed it to the effects of glacio-isostatic movements. Fault movements for this time-period were also found in later trench studies by Vandenberghe et al. (2009) for the Geleen fault, and by Van Balen et al. (2019) for the Peel Boundary fault zone at Bakel (Fig. 10), the northern boundary fault zone of the RVG. The timing of these faulting events is in agreement with independent evidence for a forebulge and its collapse based on sea-level data (Kiden et al., 2002), fluvial response of the Rhine river (Busschers et al., 2007) and glacio-isostatic modeling (e.g. Vink et al., 2007). Forebulge decay causes bending stresses which may stimulate the slip of faults, depending on their orientation and on the ambient plate-tectonic stress conditions (Muir-Wood, 2000; Hampel et al., 2009).

Glacio-isostatic movements have also been invoked before to explain earthquake events in northern Germany and Denmark (Sandersen and Jørgensen, 2014; Brandes et al., 2012, 2015, 2018, 2015; Müller et al., 2020). Remarkably, the glacio-isostatic effects on faulting did not occur during the phase of early deglaciation of the Scandinavian ice sheet (SIS) at ~19.0 ka. Instead, the timing of the faulting events is co-eval with the large-scale recession of the southern SIS margin at about 14.6 ka, which is likely a response to the abrupt onset of the Bølling-Allerød warm interval (Rinterknecht et al., 2006; Cuzzone et al., 2016; Stroeven et al., 2016). Glacio-isostasy not only impacted the timing of earthquakes. Dating results on volcanic eruptions in the nearby Eifel show that also these events are triggered by glacio-isostatic motions. The youngest series of eruptions started at around 15.5 ± 1.1 ka ago, the last event occurred 10.940 ± 90 cal BP (note, the famous Laacher See Volcano eruption dates at 12.960 ± 140 cal BP; Schmidt et al., 2017).

In addition to glacio-isostasy also plume-induced uplift likely has contributed to fault activity. Ahorner (1962) and Houtgast and Van Balen (2000) showed that fault displacement and subsidence rates in the RVRS increased during the Pleistocene. Recently, Gold et al. (2017) showed that fault displacement rates in the eastern part of the RVRS have increased since 700–800 ka, which is coeval with increased uplift rate in the adjoining Ardennes-Eifel area. This domal uplift in the Ardennes-Eifel has been attributed to the rise of a mantle plume centred at the Eifel volcanic area (Van Balen et al., 2000; Demoulin and Hallot, 2009). Recently, the link between plume-induced uplift and increased faulting activity has been evidenced by Kreemer et al. (2020) using GPS data. They were able to show that the eastern part of the RVRS experiences horizontal extension as a result of the uplift. The uplift-induced extension can thus explain the concentration of present-day seismic activity in the eastern part of the RVRS. The impact of glacio-isostatic motions on the volcanism and seismic activity is superimposed on these plume-induced effects.

5.3.3. Implications of mining-induced fault reactivation

Coal mining at depth has reactivated the upper part of the Heerlerheide fault. This implies that the fault is a zone of structural weakness. The fault has not been reactivated during reflooding of the mines and consequent surface rebound. However, that still might happen, as the rebound is still ongoing.

Our results show that not taking into account potential anthropogenic causes for fault motion could lead to erroneous interpretations. If we would not have known about the mining-induced subsidence, we would have interpreted the youngest, 0.35 m displacement as a magnitude 6.5, sub-Recent tectonic earthquake. Coal mining has taken part over a large area in the southeastern part of the RVRS, on Belgian, Dutch and German territory, and mining-induced fault reactivation is likely widespread. In addition, in the German section of the RVRS, brown-coal mining still takes place in up to 370 m deep open pit mines, which requires lowering groundwater level several hundred meters regionally and thus causing compaction subsidence and fault reactivation over large areas. In this respect, our observations for the mining-induced fault reactivation show striking similarities to the Holocene fault and fractures presented by Grützner et al. (2016) for a trench across the Rurrand fault, which they interpreted as a Holocene surface rupturing earthquake event. Their results show a fault which branches in the upper part, where colluvium with charcoal particles and ceramic fragments fill a crack, similar to our results. Because the overlying ~0.4 m thick plough zone was not affected by faulting, Grützner et al. (2016) conclude that this implies a very young tectonic displacement event. However, because normally a plough zone is continuously reworked by farmers, a continuation of the fault towards the surface could have been destroyed by ploughing.

The Holocene surface ruptures and fault displacements concluded for the Feldbiss fault and the Geleen fault trenches (see above) are likely not affected by coal mining, since the nearest mine

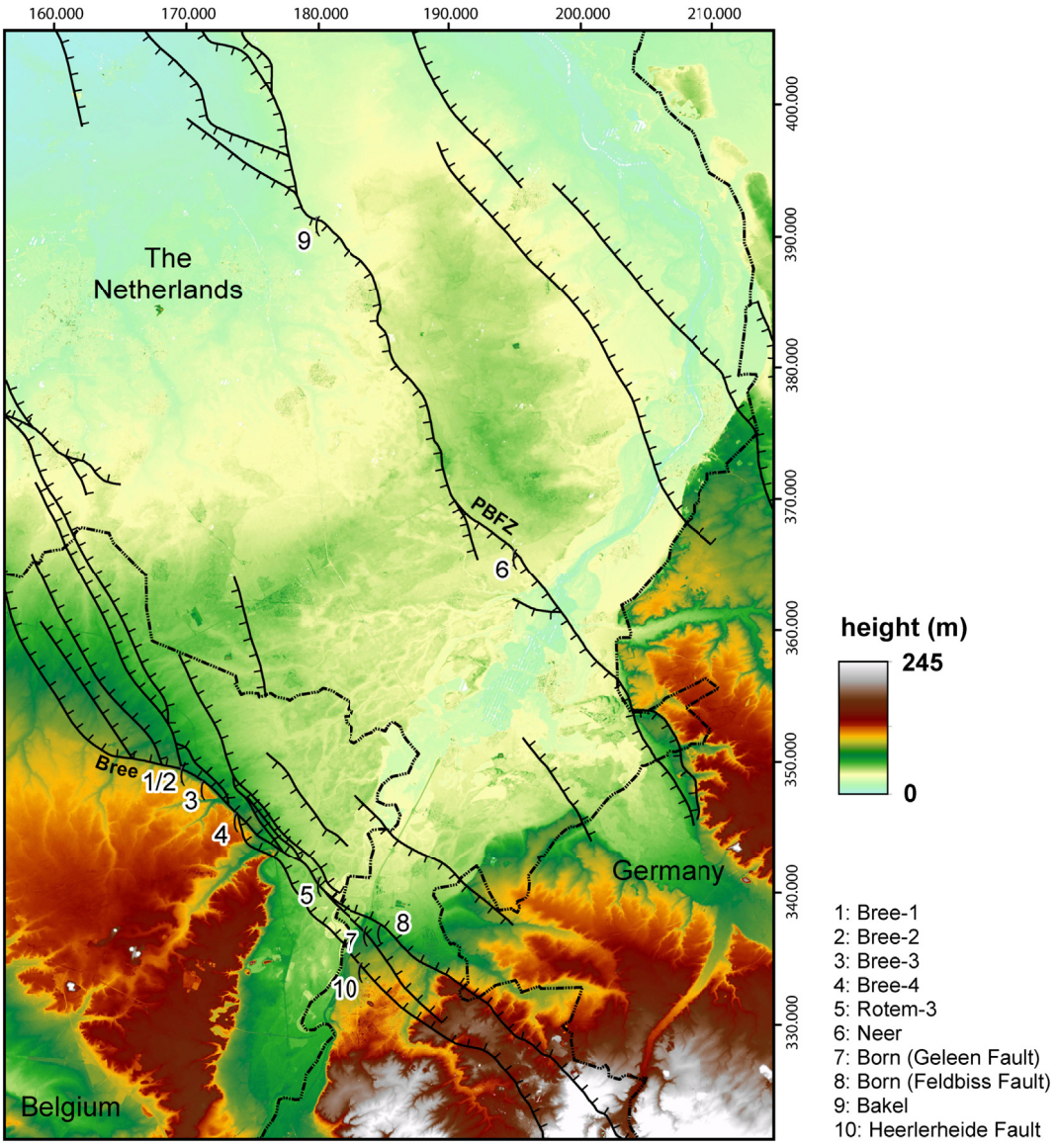

Fig. 10. The location of trenches in the RVRS where paleoearthquakes have been identified which occurred in the time window between 15 and 17 ka. PBFZ = Peel Boundary fault zone. For trenches 1, 2, 3, 4 and 5 see Vanneste et al. (2018). Trench 6 is described by Van den Berg et al. (2002), trench 7 by Houtgast et al. (2003), trench 8 by Houtgast et al. (2005), trench 9 by Van Balen et al. (2019) and trench 10 is presented in this paper. Trenches 6 and 9 are located at the Peel Boundary Fault zone, the northern boundary fault of the RVRS. All other trenches are at faults of the FFZ. See text for discussion.

shafts were more than 5 km to the south.

6. Conclusions

A trench was studied across the Heerlerheide fault of the Feldbiss fault zone. The oldest units are part of the Caberg-2 terrace, and dated at about 340 ka. The subunits of the overlying silt unit are correlated to the regional Eemian-Weichselian loess stratigraphy in western Europe. The sequence contains the well-known Eemian-Early Weichselian Rocourt soil, Kesselt layer (reworked sandy loess), Nagelbeek tongued horizon or —soil complex, and the primary Brabant loess.

The reconstructed displacement history of the Heerlerheide fault consists of at least three tectonic events and one final, more recent mining-induced displacement, see Table 2 for amounts and ages of displacements. The tectonic faulting events may have been surface rupturing earthquakes of magnitude 6.2 or more: the oldest is associated with a colluvial wedge on the terrace, the penultimate cuts sharply through the Rocourt soil, whereas the last one offsets the Late Pleniglacial loess, during the 17 to 15 ka time-interval. However, the two oldest displacements also could represent multiple faulting events. The time interval between the two youngest events is at least 8 ky. The relatively well-constrained age of the last tectonic event is correlatable to previous results for other trenches across faults of the Feldbiss fault zone in the Netherlands and in Belgium. In addition, also the most recent major surface rupturing event along the Peel Boundary fault zone has the same age. The timing is roughly contemporaneous with surface rupturing earthquakes in northern Germany and Denmark and the youngest phase of volcanism in the nearby Eifel area, indicating a common mechanism. The ages suggest that they have glacio-isostatic movements as the common driver.

Remarkably, the studied trench showed that the Heerlerheide fault experienced no Late Glacial and Holocene displacement. This

contrasts with other faults in the FFZ: The Feldbiss and Geleen fault in the Dutch part of the FFZ likely experienced 0.6 m surface rupturing, possibly between 8.1 ± 0.7 ka and 7.0 ± 0.5 ka, where in the Belgian part of the Geleen fault a ~1 m surface rupture occurred between 2.5 ± 0.3 and 3.1 ± 0.3 ka.

The coal mining-induced fault reactivation took place during the mining, and not afterwards, despite the still ongoing surface rebound after abandonment and re-flooding of the mines. In addition to faulting, the mining subsidence on the hanging wall also caused a surface gradient which, in turn, caused minor downslope movement, resulting in a crack-like splaying of the tip of the Heerlerheide fault, filled-in by plough layer material.

Author contribution

All authors have made substantial contributions to the manuscript. Van Balen and Woolderink did most of the research in the trench. Kasse helped with the stratigraphical and sedimentological interpretations. Wallinga did the luminescence analyses. Van Balen wrote the manuscript. All co-authors have helped with the writing. All authors agree with the submission.

Declaration of competing interest

There are no competing interests, not direct nor indirect. There is no undisclosed funding source, and no undisclosed relationship.

Acknowledgements

Rob Paulussen (ArcheoPro), Xavier van Dijk (RAAP) and dr Peter Rosner (IHS) are thanked for discussion during the trenching. TNO colleagues and Klaus Reicherter (RWTH Aachen) are thanked for the discussions during their site visit. We thank Benny Guralnik and Erna Voskuilen for their support in the NCL lab. We thank ir. Frank Denys (Ministry of Economic Affairs and Climate Policy, the Netherlands) for his general support. Finally, we thank Christian Brandes and Kris Vanneste for their constructive reviews.

Appendix A. Supplementary data

Supplementary data to this article can be found online at https://doi.org/10.1016/j.quascirev.2021.107111.

References

Ahorner, L., 1962. Untersuchungen zur quartären Bruchtektonik der Niederrheinischen Bucht. Eiszeitalt. Ggw. 13, 24–105.
Brandes, C., Winsemann, J., Roskoch, J., Meinsen, J., Tanner, D.C., Frechen, M., Steffen, H., Wu, P., 2012. Activity of the Osning thrust in central Europe during the Lateglacial: ice-sheet and lithosphere interactions. Quat. Sci. Rev. 38, 49–62.
Brandes, C., Steffen, H., Steffen, R., Wu, P., 2015. Intraplate seismicity in northern Central Europe is induced by the last glaciation. Geology 43, 611–614.
Brandes, C., Steffen, H., Sandersen, P.B.E., Wu, P., Winsemann, J., 2018. Glacially induced faulting along the NW segment of the Sorgenfrei-Tornquist Zone, northern Denmark: implications for neotectonics and Lateglacial fault-bound basin formation. Quat. Sci. Rev. 189, 149–168.
Busschers, F.S., Kasse, C., Van Balen, R.T., Vandenberghe, J., Cohen, K.M., Weerts, H.J.T., Wallinga, J., Johns, C., Cleveringa, P., Bunnik, F.P.M., 2007. Late Pleistocene evolution of the Rhine in the southern North-Sea Basin: imprints of climate change, sea-level oscillations and glacio-isostacy. Quat. Sci. Rev. 26, 3216–3248.
Camelbeeck, T., Vanneste, K., Alexandre, P., Verbeeck, K., Petermans, T., Rosset, P., Everaerts, M., Warnant, R., Van Camp, M., 2007. Relevance of active faulting and seismicity studies to assessments of long-term earthquake activity and maximum magnitude in intraplate northwest Europe, between the Lower Rhine Embayment and the North Sea. In: Stein, S., Mazzotti, S. (Eds.), Continental Intraplate Earthquakes: Science, Hazard and Policy Issues, vol. 425. Geological Society of America Special Paper, pp. 193–224.
Caro Cuenca, M., Hooper, A.J., Hansen, R.F., 2013. Surface deformation induced by water influx in the abandoned coal mines in Limburg, The Netherlands. J. Appl. Geophys. 88, 1–11.
Cunningham, A.C., Wallinga, J., 2010. Selection of integration time-intervals for quartz OSL decay curves. Quat. Geochronol. 5, 657–666.
Cuzzone, J.K., Clark, P.U., Carlson, A.E., Ullman, D.J., Rinterknecht, V.R., Milned, G.A., Lunkka, J.P., Wohlfarth, B., Marcott, S.A., Caffee, M., 2016. Final deglaciation of the Scandinavian Ice Sheet and implications for the Holocene global sea-level budget. Earth Planet Sci. Lett. 448, 34–41.
Deckers, J., Rombaut, B., Van Noten, K., Vanneste, K., 2021. Influence of inherited structural domains and their particular strain distributions on the Roer Valley graben evolution from inversion to extension. J. Geoph. Res. - Solid Earth 12, 345–361. https://doi.org/10.5194/se-12-345-2021.
Demoulin, A., Hallot, E., 2009. Shape and amount of the Quaternary uplift of the western Rhenish shield and the Ardennes (western Europe). Tectonophysics 474, 696–708.
Galbraith, R.F., Roberts, R.G., Laslett, G.M., Yoshida, H., Olley, J.M., 1999. Optical dating of single and multiple grains of quartz from Jinmium Rock Shelter, northern Australia: Part I, experimental design and Statistical models. Archaeometry 41, 339–364.
Geluk, M.C., Duin, E.J., Dusar, M., Rijkers, R., Van den Berg, M.W., Van Rooijen, P., 1994. Stratigraphy and tectonics of the Roer Valley graben. Neth. J. Geosci. - Geol. Mijnb. 73, 129–141.
Gold, R.D., Friedrich, A., Kübler, S., Salamon, M., 2017. Apparent late quaternary fault-slip rate increase in the southern lower rhine graben, central Europe. Bull. Seismol. Soc. Am. 107, 563–580.
Grützner, C., Fischer, P., Reicherter, K., 2016. Holocene surface ruptures of the Rurrand Fault, Germany—insights from palaeoseismology, remote sensing and shallow geophysics. Geophys. J. Int. 204, 1662–1677.
Haesaerts, P., Mestdagh, H., Bosquet, D., 1999. The sequence of Remicourt (Hesbaye, Belgium): new insights of the pedo- and chronostratigraphy of the Rocourt Soil. Geol. Belg. 2, 5–27.
Haesaerts, P., Damblon, F., Gerasimenko, N., Spagna, P., Pirson, S., 2016. The Late Pleistocene loess-palaeosol sequence of Middle Belgium. Quat. Int. 411, 25–43. https://doi.org/10.1016/j.quaint.2016.02.012.
Hampel, A., Hetzel, R., Maniatis, G., Karow, T., 2009. Three-dimensional numerical modeling of slip rate variations on normal and thrust fault arrays during ice cap growth and melting. J. Geophys. Res. - Solid Earth 114, B08406. https://doi.org/10.1029/2008JB006113.
Heiri, O., Lotter, A.F., Lemcke, G., 2001. Loss on ignition as a method for estimating organic and carbonate content in sediments: reproducibility and comparability of results. J. Paleolimnol. 25 (1), 101–110. https://doi.org/10.1023/A:1008119611481.
Heitfeld, M., Rosner, P., Pietralla, S., Rosin, D., 2016. Na-ijlende gevolgen steenkolenwinning zuid-Limburg. Final Report on the Results of the Working Group 5.2.1. – Ground Movements, Parts C and D, pp. 148–210 available from: https://www.tweedekamer.nl/kamerstukken/detail?id=2016D49345&did=2016D49345.
Heitfeld, M., Rosner, P., Pietralla, S., 2018. Pilot Projet No. 3 – Geleen. Report about the Exposure of the Heerlerheide Fault in an Excavated Trench – On-Site Investigation and Risk Assessment, p. 139.
Houtgast, R.F., Van Balen, R.T., 2000. Neotectonics of the Roer Valley Rift System, The Netherlands. Global Planet. Change 27, 131–146.
Houtgast, R.F., Van Balen, R.T., Bouwer, L.M., Brand, G.B.M., Brijker, J.M., 2002. Late quaternary activity of the Feldbiss fault zone, Roer Valley rift system, The Netherlands, based on displaced fluvial terrace fragments. Tectonophysics 352, 295–315.
Houtgast, R.F., Van Balen, R.T., Kasse, C., Vandenberghe, J., 2003. Late quaternary tectonic evolution and postseismic near surface fault displacements along the Geleen fault (Feldbiss fault zone – Roer Valley rift system, The Netherlands), based on trenching. Neth. J. Geosci. - Geologie Mijnb. 82, 177–196.
Houtgast, R.F., Van Balen, R.T., Kasse, C., 2005. Late quaternary evolution of the Feldbiss fault (Roer Valley rift system, The Netherlands) based on trenching, and its potential relation to glacial unloading. Quat. Sci. Rev. 24, 491–510.
Huxtable, J., Aitken, J., 1985. Thermoluminescence dating results for the palaeolithic site maastricht –belvédère. Meded. Rijks Geol. Dienst 39, 41–44.
Johnsen, S.J., Dahl-Jensen, D., Gundestrup, N., Steffensen, J.P., Clausen, H.B., Miller, H., Masson-Delmotte, V., Sveinbjörnsdottir, A.E., White, J., 2001. Oxygen isotope and paleotemperature records from six Greenland ice-core stations: camp Century, Dye-3, GRIP, GISP2, Renland and NorthGRIP. J. Quat. Sci. 16, 299–307.
Jongmans, A.G., Van den Berg, M.W., Sonneveld, M.P.W., Peek, G.J.W.C., Van den Berg van Saparoea, R.M., 2013. Landschappen Van Nederland. Wageningen Academic Publishers, p. 942.
Juvigné, E.H., Wintle, A.G., 1988. A new chronostratigraphy of the Late Weichselian loess units in Middle Europe based on thermoluminescence dating. Eiszeitalt. Ggw. 38, 95–105.
Kars, R.H., Busschers, F.S., Wallinga, J., 2012. Validating post IRIRSL dating on K-feldspars through comparison with quartz OSL ages. Quat. Geochronol. 12, 74–86.
Kiden, P., Denys, L., Johnston, P., 2002. Late Quaternary sea-level change and isostatic and tectonic land movements along the Belgian-Dutch North Sea coast: geological data and model results. J. Quat. Sci. 17, 535–546.
Konert, M., Vandenberghe, J., 1997. Comparison of laser grains size analysis with pipette and sieve analysis: a solution for the underestimation of the clay fraction. Sedimentology 44, 523–535.
Kreemer, C., Blewitt, G., Davis, P.M., 2020. Geodetic evidence for a buoyant mantle plume beneath the Eifel volcanic area, NW Europe. Geophys. J. Int. 222,

1316–1332.
Kübler, S., Streich, R., Lück, E., Hoffmann, M., Friedrich, A., Strecker, M., 2017. Active faulting in a populated low-strain setting (Lower Rhine Graben, Central Europe) identified by geomorphic, geophysical and geological analysis, 432. Geological Society, London, Special Publications, pp. 127–146. https://doi.org/10.1144/SP432.11.
Lehmkuhl, F., Zens, J., Krauß, L., Schulte, P., Kels, H., 2016. Loess-paleosol sequences at the northern European loess belt in Germany: distribution, geomorphology and stratigraphy. Quat. Sci. Rev. 153, 11–30.
Meijs, E.P.M., 2002. Loess stratigraphy in Dutch and Belgian limburg. Eiszeitalt. Ggw. 51, 114–130.
Meijs, E.P.M., 2011. The Veldwezelt site (province of Limburg, Belgium): environmental and stratigraphical interpretations. Neth. J. Geosci. – Geol. Mijnb. 90, 73–94.
Meijs, E.P.M., Van Peer, Ph, De Warrimont, J.P.L.M.N., 2012. Geomorphic context and proposed chronostratigraphic position of Lower Paleolithic artefacts from the Op de Schans pit near Kesselt (Belgium) to the west of Maastricht. Neth. J. Geosci. – Geol. Mijnb. 91, 137–157.
Michon, L., Van Balen, R.T., Merle, O., Pagnier, H., 2003. Cenozoic evolution of the Roer Valley rift system integrated at European scale. Tectonophysics 367, 101–126.
Michon, L., Van Balen, R.T., 2005. Characterization and quantification of active faulting in the Roer valley rift system based on high precision digital elevation models. Quat. Sci. Rev. 24, 457–474.
Muir-Wood, R., 2000. Deglaciation seismotectonics: a principal influence on intraplate seismogenesis at high latitudes. Quat. Sci. Rev. 19, 1399–1411.
Müller, K., Polom, U., Winsemann, J., Stefen, H., Tsukamoto, S., Günther, T., Igel, J., Spies, T., Lege, T., Frechen, M., Franzke, H., Brandes, C., 2020. Structural style and neotectonic activity along the Harz Boundary Fault, northern Germany: a multimethod approach integrating geophysics, outcrop data and numerical simulations. Int. J. Earth Sci. 109, 1811–1835. https://doi-org.vu-nl.idm.oclc.org/10.1007/s00531-020-01874-0.
Murray, A.S., Wintle, A.G., 2003. The single aliquot regenerative dose protocol:potential for improvements in reliability. Radiat. Meas. 37, 377–381.
Porat, N., 2006. Use of magnetic separation for purifying quartz for luminescence dating. Ancient TL 24, 33–36.
Pöttgens, J.J.E., 1985. Bodenhebung durch ansteigendes Grubenwasser. The developing science and art of minerals surveying. Proceedings of the 6th International Congress for Mine Surveying, Harrogate, pp. 928–938.
Pouclet, A., Juvigne, E., 2009. The Eltville tephra, a late Pleistocene widespread tephra layer in Germany, Belgium and The Netherlands; symptomatic compositions of the minerals. Geol. Belg. 12, 93–103.
Reimer, P.J., Bard, E., Bayliss, A., Beck, J.W., Blackwell, P.G., Bronk Ramsey, C., Buck, C.E., Cheng, H., Edwards, R.L., Freidrich, M., Grootes, P.M., Guilderson, T.P., Haflidason, H., Hajdas, I., Hatte, C., Heaton, T.J., Hoffmann, D.G., Hogg, A.G., Hughen, K.A., Kaiser, K.F., Kromer, B., Manning, S.W., Nui, M., Reimer, R.W., Richards, R.A., Scott, E.M., Southon, J.R., Staff, R.A., Turney, C.M.S., Van der Plicht, J., 2013. IntCal13 and Marine13 calibration curves 0-50,000 Years BP. Radiocarbon 55 (4), 1869–1887.
Rhodes, E.J., 2011. Optically stimulated luminescence dating of sediments over the past 200,000 Years. Annu. Rev. Earth Planet Sci. 39, 461–488. https://doi.org/10.1146/annurev-earth-040610-133425.
Rinterknecht, V.R., Clark, P.U., Raisbeck, G.M., Yiou, F., Bitinas, A., Brook, E.J., Marks, L., Zelcs, V., Lunkka, J.-P., Pavlovskaya, I.E., Piotrowski, J.A., Raukas, A., 2006. The last deglaciation of the southeastern sector of the scandinavian ice sheet. Science 311, 1449–1452.
Ruijters, M.H.P.M., Ellenkamp, G.R., Tichelman, G., 2015. De beek die geeft en de beek die neemt. RAAP-RAPPORT 2989. RAAP Archeologisch Adviesbureau BV, p. 305.
Sandersen, P.B., Jørgensen, F., 2014. Neotectonic deformation of a Late Weichselian outwash plan by deglacation-induced fault reactivation of a deep-seated graben structure. Boreas 44, 413–431.
Schirmer, W., 2016. Late Pleistocene loess of the lower rhine. Quat. Int. 411, 44–61.
Schmidt, C., Schaarschmidt, M., Kolb, T., Büchel, G., Richter, D., Zöller, L., 2017. Luminescence dating of Late Pleistocene eruptions in the Eifel volcanic field, Germany. J. Quat. Sci. 32, 628–638.
Stroeven, A.P., Hättestrand, C., Kleman, J., Heyman, J., Fabel, D., Fredian, O., Goodfellow, B.M., Harbor, J.M., Jansen, J.D., Olsen, L., Caffee, M.W., Fink, D., Lundqvist, J., Rosqvist, G.C., Strömberg, B., Jansson, K.N., 2016. Deglaciation of fennoscandia. Quat. Sci. Rev. 147, 91-21.
Thiel, C., Buylaert, J.P., Murray, A., Terhorst, B., Hofer, I., Tsukamoto, S., Frechen, M., 2011. Luminescence dating of the Stratzing loess profile (Austria) - testing the potential of an elevated temperature post-IR IRSL protocol. Quat. Int. 234 (1–2), 23–31. https://doi.org/10.1016/j.quaint.2010.05.018.
Van Balen, R.T., Houtgast, R.F., Van der Wateren, F.M., Vandenberghe, J., Bogaart, P.W., 2000. Sediment budget and tectonic evolution of the Meuse catchment in the Ardennes and the Roer Valley rift system. Global Planet. Change 27, 113–130.
Van Balen, R.T., Houtgast, R.F., Cloetingh, S.A.P.L., 2005. Neotectonics of The Netherlands. Quat. Sci. Rev. 24, 439–454.
Van Balen, R.T., Bakker, M.A.J., Kasse, C., Wallinga, J., Woolderink, H., 2019. A late glacial surface rupturing earthquake at the Peel boundary Fault zone, Roer Valley rift system, The Netherlands. Quat. Sci. Rev. 218, 254–266.
Van den Berg, M.W., 1996. Fluvial Sequences of the Maas, a 10 Ma Record of Neotectonics and Climate Change at Various Timescales. PhD thesis, Universiteit Wageningen, p. 181.
Van den Berg, M.W., Van Hoof, T., 2001. The Maas terrace sequence at Maastricht, SE Netherlands: evidence for 200 m of late Neogene and Quaternary surface uplift. In: Maddy, D., Macklin, M.G., Woodward, J.C. (Eds.), River Basin Sediment Systems: Archives of Environmental Change. A.A. Balkema Publishers, Lisse, pp. 45–86.
Van den Berg, M., Vanneste, K., Dost, B., Lokhorst, A., Van Eijk, M., Verbeeck, K., 2002. Paleoseismic investigations along the Peel Boundary Fault: geological setting, site selection and trenching results. Neth. J. Geosci. – Geol. Mijnb. 81, 39–60.
Vandenberghe, D., Vanneste, K., Verbeeck, K., Paulissen, E., Buylaert, J.P., De Corte, F., Van den Haute, P., 2009. Late Weichselian and Holocene earthquake events along the Geleen fault in NE Belgium: OSL age constraints. Quat. Int. 199, 56–74.
Van Eck, T., Davenport, C.A., 1994. Seismotectonics and seismic hazard in the Roer Valley graben; with emphasis on the Roermond earthquake of april 13, 1992, geol. Mijnbouw 73, 91–92.
Van Kolfschoten, T., Roebroeks, W., Vandenberghe, J., 1993. The middle and late Pleistocene sequence at maastricht– belvédère: the type locality of the belvédère interglacial. Meded. – Rijks Geol. Dienst, Nieuwe Ser. 47, 81–91.
Vanneste, K., Camelbeeck, T., Verbeeck, K., Demoulin, A., 2018. Morphotectonics and past large earthquakes in eastern Belgium. In: Demoulin, A. (Ed.), Landscapes and Landforms of Belgium and Luxembourg. World Geomorphological Landscapes, pp. 215–236. https://doi.org/10.1007/978-3-319-58239-9_13.
Vervoort, A., 2016. Surface movement above an underground coal longwall mine after closure, Nat. Hazards Earth Syst. Sci. 16, 2107–2121.
Vink, A., Steffen, H., Reinhardt, L., Kaufmann, G., 2007. Holocene relative sea-level change, isostatic subsidence and the radial viscosity structure of the mantle of northwest Europe (Belgium, The Netherlands, Germany, southern north Sea). Quat. Sci. Rev. 26, 3249–3275.
Vis, G.J., Van Linden, E., Van Balen, R., Cohen, K., 2020. Depressions caused by localized subsidence in The Netherlands, Belgium and Germany: a link with coal mining? Proceedings of the e International Association of Hydrological Sciences 382, 201–205. https://doi.org/10.5194/piahs-382-201-2020.
Wells, D.L., Coppersmith, K.J., 1994. New empirical relationships among magnitude, rupture length, rupture width, rupture area, and surface displacement. Bulletin of the Seismological Society of America, pp. 974–1002.
Yavuz, H., 2004. An estimation method for cover pressure re-establishment distance and pressure distribution in the goaf of longwall coal mines. Int. J. Rock Mech. Min. Sci. 41, 193–205.
Zens, J., Zeeden, C., Römer, W., Guchs, M., Klasen, N., Lehmkuhl, F., 2017. The Eltville Tephra (Western Europe) age revised: integrating stratigraphic and dating information from different Last Glacial loess localities. Paleogeography, Paleoclimatology, Paleoecology 466, 240–251.
Zens, J., Schulte, P., Klasen, N., Krauß, L., Pirson, S., Burow, C., Brill, D., Eckmeier, E., Kels, H., Zeeden, C., Spagna, P., Lehmkuhl, F., 2018. OSL chronologies of paleoenvironmental dynamics recorded by loess paleosol sequences from Europe: case studies from the Rhine-Meuse area and the Neckar Basin. Palaeogeogr. Palaeoclimatol. Palaeoecol. 509, 105–125. https://doi.org/10.1016/j.palaeo.2017.07.019.
Ziegler, P.A., 1992. European Cenozoic rift system. Tectonophysics 208, 91–111.